1521-009X/51/3/369–384$35.00
DRUG METABOLISM AND DISPOSITION
dx.doi.org/10.1124/dmd.122.000853
Drug Metab Dispos 51:369–384, March 2023

50th Anniversary Celebration Collection

Special Section on Drug Metabolism and Precision Medicine—Minireview

Multidisciplinary Insights into the Structure–Function Relationship of the CYP2B6 Active Site[S]

Ethan D. Angle and Philip M. Cox

Department of Biology and Chemistry, College of Liberal Arts and Sciences, Azusa Pacific University, Azusa, California (E.D.A., P.M.C.) and Roy J. and Lucille A. Carver College of Medicine University of Iowa, Iowa City, Iowa (E.D.A.)

Received January 30, 2022; accepted November 4, 2022

ABSTRACT

Cytochrome P450 2B6 (CYP2B6) is a highly polymorphic human enzyme involved in the metabolism of many clinically relevant drugs, environmental toxins, and endogenous molecules with disparate structures. Over the last 20-plus years, in silico and in vitro studies of CYP2B6 using various ligands have provided foundational information regarding the substrate specificity and structure–function relationship of this enzyme. Approaches such as homology modeling, X-ray crystallography, molecular docking, and kinetic activity assays coupled with CYP2B6 mutagenesis have done much to characterize this originally neglected monooxygenase. However, a complete understanding of the structural details that make new chemical entities substrates of CYP2B6 is still lacking. Surprisingly little in vitro data has been obtained about the structure–function relationship of amino acids identified to be in the CYP2B6 active site. Since much attention has already been devoted to elucidating the function of CYP2B6 allelic variants, here we review the salient findings of in silico and in vitro studies of the CYP2B6 structure–function relationship with a deliberate focus on the active site. In addition to summarizing these complementary approaches to studying structure–function relationships, we note gaps/challenges in existing data such as the need for more CYP2B6 crystal structures, molecular docking results with various ligands, and data coupling CYP2B6 active site mutagenesis with kinetic parameter measurement under standard expression conditions. Harnessing in silico and in vitro techniques in tandem to understand the CYP2B6 structure–function relationship will likely offer further insights into CYP2B6-mediated metabolism.

SIGNIFICANCE STATEMENT

The apparent importance of cytochrome P450 2B6 (CYP2B6) in the metabolism of various xenobiotics and endogenous molecules has grown since its discovery with many in silico and in vitro studies offering a partial description of its structure–function relationship. Determining the structure–function relationship of CYP2B6 is difficult but may be aided by thorough biochemical investigations of the CYP2B6 active site that provide a more complete pharmacological understanding of this important enzyme.

Introduction

The cytochromes P450 (P450) are a superfamily of heme-containing monooxygenases found in all kingdoms of life (Nelson, 2011). P450s participate in the metabolism of xenobiotics, such as clinically relevant drugs and environmental toxins (Guengerich, 2017), as well as endogenous compounds, including eicosanoids, vitamins, and steroid hormones (Nebert et al., 2013). As the only expressed member of the human 2B subfamily, cytochrome P450 2B6 (CYP2B6) has been the subject

This work received no external funding.

No author has an actual or perceived conflict of interest with the contents of this article.

dx.doi.org/10.1124/dmd.122.000853.

[S] This article has supplemental material available at dmd.aspetjournals.org.

ABBREVIATIONS: BDE-47, 2,2',4,4'-tetrabromodiphenyl ether; 3-OH-BDE-47, 3-hydroxy-2,2′,4,4′-tetrabromodiphenyl ether; 5-OH-BDE-47, 5-hydroxy-2,2',4,4'-tetrabromodiphenyl ether; 6-OH-BDE-47, 6-hydroxy-2,2',4,4'-tetrabromodiphenyl ether; 4'-OH-BDE-49, 4'-hydroxy-2,2',4,5′-tetrabromodiphenyl ether; BDE-99, 2,2',4,4',5-pentabromodiphenyl ether; BDE-100, 2,2',4,4',6-pentabromodiphenyl ether; 3-OH-BDE-100, 3-hydroxy-2,2',4,4', 6-pentabromodiphenyl ether; 3′-OH-BDE-100, 3′-hydroxy-2,2',4,4',6-pentabromodiphenyl ether; 5′-OH-BDE-100, 5′-hydroxy-2,2',4,4',6-pentabromodiphenyl ether; 6'-OH-BDE-100, 6'-hydroxy-2,2',4,4',6-pentabromodiphenyl ether; BPA, 4-*tert*-butylphenylacetylene; 4-BP, 4-benzylpyridine; CB118, 2,3′,4,4',5-pentachlorobiphenyl; 4-CPI, 4-(4-chlorophenyl)imidazole; CYP2B1, cytochrome P450 2B1; CYP2B4, cytochrome P450 2B4; CYP2B6, cytochrome P450 2B6; CYP2E1, cytochrome P450 2E1; Cyt b5, cytochrome b5; 7-EFC, 4-trifluoromethyl-7-ethoxycoumarin; 4-NBP, 4-(4-nitrobenzyl)pyridine; OCDD, 1,2,3,4,6,7,8,9-octachlorodibenzo-*p*-dioxin; P450, cytochrome P450; PBDE, polybrominated diphenyl ether; PCB, polychlorinated biphenyl; PCB-187, 2,2',3,4',5,5′,6-heptachlorobiphenyl; PDB, Protein Data Bank; POA, phenoxyaniline; POR, P450 oxidoreductase; QSAR, quantitative structure–activity relationship; RP 73401 or Piclamilast, 3-cyclopentyloxy-*N*-(3,5-dichloro-4-pyridyl)-4-methoxybenzamide; SRS, substrate recognition site; WZ35, 1-(4-hydroxy-3-methoxyphenyl)-5-(2-nitrophenyl)penta-1,4-dien-3-1.

of experimental interest since its discovery in the late 1980s (Miles et al., 1988) due to its primary role in the metabolism of clinically important drugs (e.g., efavirenz, bupropion, methadone, ketamine, and cyclophosphamide) in addition to its extensive polymorphism (Zanger and Klein, 2013; Desta et al., 2021). As more CYP2B6 substrates were identified, there was a growing interest in characterizing *how* and *why* the active site structure of CYP2B6 functions in coordinated, substrate-specific oxidative catalysis with the eventual goal of computationally screening the metabolic profile of new chemical entities(Lewis, 1999; Lewis et al., 1999).

The computational power of predicting enzymatic structure–function relationships has grown within the last 20 years. Specifically, a surplus of in silico information concerning CYP2B6 such as its substrate/inhibitor characteristics (Wang and Halpert, 2002; Korhonen et al., 2007; Ekins et al., 2008; Wang et al., 2019b), 13 crystal structures Table 1), active site amino acids (Supplemental Table 1 and Table 1), and plasticity (Shah et al., 2012; Wilderman and Halpert, 2012; Shah et al., 2018) has been elucidated. The techniques of quantitative structure–activity relationships (QSARs) (Wang and Halpert, 2002; Lewis et al., 2010; Dmitriev et al., 2021), homology modeling (Lewis et al., 1999; Bathelt et al., 2002; Lewis et al., 2002), X-ray crystallography (Gay et al., 2010; Halpert, 2011; Shah et al., 2018), and molecular docking (Niu et al., 2011; Radloff et al., 2013; Maldonado-Rojas et al., 2016) have been pivotal in this endeavor. For a full view of the significant in silico work done with CYP2B6, we have compiled a historical table of CYP2B6 homology models (Supplemental Table 1) and a modern table of CYP2B6 crystal structures/molecular docking results (Table 1) with predicted active site residues around various ligands noted. The in silico information collected through these techniques will be reviewed herein to exemplify advancements in the field of assessing the CYP2B6 structure–function relationship. However, in vitro activity data measuring the kinetics of CYP2B6 are also of utmost importance to these advancements.

Most studies investigating CYP2B6 kinetics have been more focused on identifying substrates of this enzyme than venturing deeper into its structure–function relationship. As a result, the in vitro insights reviewed here will underscore the subset of those exploring CYP2B6 mutagenesis (Domanski et al., 1999; Spatzenegger et al., 2003; Nguyen et al., 2008; Lin et al., 2016), substrate moiety modulation (Cox and Bumpus, 2014; Cox and Bumpus, 2016; Liu et al., 2016; Wang et al., 2019b), and substrate/stereo-/regio-specificity (Roy et al., 1999; Totah et al., 2007; Erratico et al., 2015; Wang et al., 2018; Wang et al., 2019a). CYP2B6 mutagenesis has largely been performed to better understand the metabolic activity of allelic variants, which is thoroughly reviewed elsewhere (Zanger et al., 2007; Wang and Tompkins, 2008; Mo et al., 2009; Turpeinen and Zanger, 2012; Zanger and Klein, 2013; Naidoo et al., 2014; Langmia et al., 2021). Despite their pharmacological interest, these studies do not necessarily advance our understanding of the CYP2B6 active site and will not be explored here. Thus, reports performing mutagenesis to characterize CYP2B6 active site residues will be reviewed here for the first time. We have tabulated kinetic parameters for every published CYP2B6 active site mutant (Table 2) and the problematic expression system-dependence of CYP2B6 kinetic parameters that has permeated the in vitro work of the field (Table 3). Analyzing CYP2B6 substrates will be prioritized over inhibitors with the discussion of their K_m and k_{cat} (Table 2) to highlight meaningful biochemical insights into the structure–function relationship of the CYP2B6 active site.

Our current understanding of the CYP2B6 structure–function relationship has benefitted from in silico and in vitro data. Previous in silico work identifying six substrate recognition sites (SRSs) in P450 family 2 has been helpful to note where amino acids involved in CYP2B6 substrate binding are likely located (Gotoh, 1992), but this and further information specific to CYP2B6 that has been elucidated in silico has not been thoroughly assessed in vitro (Table 2). Multidisciplinary studies utilizing in silico and in vitro techniques can provide hypothesis-generating information about the CYP2B6 active site and, by extension, shed further light on the CYP2B6 structure–function relationship.

In Silico Insights

Characterizing CYP2B6 Ligands. Early QSARs postulated that CYP2B6 ligands possess two (Wang and Halpert, 2002) to three (Ekins et al., 1999) hydrophobes and one (Ekins et al., 1999; Lewis, 2000; Wang and Halpert, 2002) to two (Lewis, 2000) hydrogen bond acceptor region(s). More general descriptors for CYP2B6 ligands have indicated the importance of nonplanarity, high volume, moderate molar mass, positive electrostatic potential, neutrality/weak basicity, hydrogen bond acceptor capacity, and, most importantly, high lipophilicity with a canonical "butterfly-wing conformation" (Ekins et al., 1999; Lewis, 2000; Lewis et al., 2001; Wang and Halpert, 2002; Appiah-Opong et al., 2008; Lewis et al., 2010). The hydrophobicity of CYP2B6 ligands is usually supplied by one or more aromatic rings (Lewis et al., 2002), their weak basicity coincides with the presence of protonatable nitrogen(s), and the number of hydrogen bond donors in the CYP2B6 active site is a limiting factor for the number of hydrogen bonds formed when binding ligands (Lewis et al., 2001; Lewis, 2003). The average molar mass of CYP2B6 ligands is about 250 to 300 g/mol, and, as more substrates were identified, each has about 2.5 hydrogen bond acceptors (Ekins et al., 2008). The nonplanarity of CYP2B6 ligands is evidenced by rotatable heterocyclic rings (Korhonen et al., 2007) and the ease of mapping substrates within a two-dimensional template to predict oxidation sites (Koyama and Yamazoe, 2011). While this description of CYP2B6 ligands is useful, many of these characterizations are generalizations due to the sensitivity and variability of the CYP2B6 structure–function relationship. For example, CYP2B6 has difficulty metabolizing planar molecules, yet planar dioxins have been predicted to readily bind and bioaccumulate within the enzyme (Maldonado-Rojas et al., 2016). This observation can be explained, at least in part, by the capacity of halogen atoms in dioxins, other persistent organic pollutants, and additional CYP2B6 substrates/inhibitors to promote tight ligand binding within CYP2B6 (Korhonen et al., 2007; Maldonado-Rojas et al., 2016; Wang et al., 2019b).

Crystallographic Advances with CYP2B6. For many years heterologous expression and purification of CYP2B6 was challenging due in part to the existence of the N-terminal anchor embedded in the cytoplasmic surface of the endoplasmic reticulum. Scott et al. first discovered that N-terminal truncation and mutation of CYP2B6 could facilitate increased expression and solubility in E. coli (Scott et al., 2001). Crystallization of CYP2B6 remained elusive until Bumpus et al. demonstrated the utility of the K262R polymorphic variant for increased solubility into cytosolic fractions (Bumpus et al., 2005). The Halpert Laboratory additionally found the Y226H mutation to further favor CYP2B6 crystallization and successfully solved the first CYP2B6 structure as an N-terminally truncated Y226H/K262R double mutant complexed with 4-(4-chlorophenyl) imidazole (4-CPI) (Gay et al., 2010). To date, 13 crystal structures of CYP2B6 in complex with 11 unique ligands above the heme prosthetic group have been solved through the utilization of N-terminal truncation and the Y226H/K262R double mutation (Table 1). Two of these structures also contain additional point mutations: I114V (Shah et al., 2017) and Y244W (Liu et al., 2016). Amino acids within 5 Å of complexed/docked ligands are canonically considered to be those pertinent for influencing the binding, orientation, and potential metabolism of the ligand (Lewis et al., 1999; Wang and Halpert, 2002; de Graaf et al., 2005; Mise et al., 2016; Hirakawa et al., 2018). Residues observed to

TABLE 1

CYP2B6 active site amino acids surrounding various ligands bound during crystallization or molecular docking experiments

Bolded and underlined entries correspond to results based on solved CYP2B6 crystal structures. Normal font entries correspond to results based on molecular docking utilizing the indicated CYP2B6 PDB ID. Residues within 5 Å of the bound ligand (proximal to the heme prosthetic group) were considered to be located in the active site.

Bound ligand PDB ID (reference)	Active site residues[a]														
	K100	I101	V104	P106	F108	Y111	I114	F115	A116	N117	F206	I209	S210	S294	F297
Amlodipine 3UA5 (Shah et al., 2012)		**X**					**X**	**X**			**X**	**X**	**X**		**X**
4-benzylpyridine 3QOA (Shah et al., 2011)		**X**	**X**				**X**	**X**			**X**	**X**			**X**
Bornane 5UDA (Shah et al., 2017)		**X**					**X**	**X**			**X**			**X**	**X**
Bornyl bromide 5UAP (Shah et al., 2017)		**X**			**X**		**X**	**X**			**X**			**X**	**X**
(+)-3-carene 4RRT (Shah et al., 2015)		**X**					**X**	**X**			**X**	**X**			**X**
4-(4-chlorophenyl)imidazole 3IBD (Gay et al., 2010)		**X**					**X**				**X**	**X**			**X**
Efavirenz 2-desoxo-2-methyl 5WBG (Shah et al., 2018)		**X**			**X**		**X**	**X**			**X**			**X**	**X**
(-)-myrtenyl bromide 5UEC (Shah et al., 2017)		**X**					**X**	**X**			**X**			**X**	**X**
(-)-myrtenyl bromide 5UFG[d] (Shah et al., 2017)		**X**			**X**		**X**[e]	**X**			**X**			**X**	**X**
4-(4-nitrobenzyl)pyridine 3QU8 (Shah et al., 2011)		**X**	**X**		**X**		**X**	**X**			**X**	**X**			**X**
(+)-α-pinene 4I91 (Wilderman et al., 2013)		**X**					**X**	**X**			**X**			**X**	**X**
(+)-α-pinene 4ZV8[c] (Liu et al., 2016)		**X**					**X**	**X**			**X**			**X**	**X**
Sabinene 4RQL (Shah et al., 2015)		**X**			**X**		**X**	**X**			**X**	**X**			**X**
2,2',4,4'-tetrabromodiphenyl ether (BDE-47) 3IBD (Zhang et al., 2021)		X									X	X			X
BDE-47 3UA5 (Maldonado-Rojas et al., 2016)		X					X	X			X				
3-hydroxy-2,2′,4,4′-tetrabromodiphenyl ether (3-OH-BDE-47) 3UA5 (Maldonado-Rojas et al., 2016)		X					X	X			X				
5-hydroxy-2,2′,4,4′-tetrabromodiphenyl ether (5-OH-BDE-47) 3UA5 (Maldonado-Rojas et al., 2016)		X	X				X	X			X	X			
6-hydroxy-2,2′,4,4′-tetrabromodiphenyl ether (6-OH-BDE-47) 3UA5 (Maldonado-Rojas et al., 2016)		X					X	X			X				X
2,2',4,4',5-pentabromodiphenyl ether (BDE-99) 3UA5 (Maldonado-Rojas et al., 2016)		X					X	X							
2,2',4,4',6-pentabromodiphenyl ether (BDE-100) 3UA5 (Maldonado-Rojas et al., 2016)		X					X	X			X				X
3-hydroxy-2,2',4,4',6-pentabromodiphenyl ether (3-OH-BDE-100) 3UA5 (Maldonado-Rojas et al., 2016)		X					X	X			X				X
3′-hydroxy-2,2',4,4',6-pentabromodiphenyl ether (3′-OH-BDE-100) 3UA5 (Maldonado-Rojas et al., 2016)		X					X	X			X				X
5′-hydroxy-2,2',4,4',6-pentabromodiphenyl ether (5′-OH-BDE-100) 3UA5 (Maldonado-Rojas et al., 2016)		X					X	X			X				X
6'-hydroxy-2,2',4,4',6-pentabromodiphenyl ether (6'-OH-BDE-100) 3UA5 (Maldonado-Rojas et al., 2016)		X					X	X			X				X
Bromoketamine 3IBD (Wang et al., 2019b)		X					X				X				X
Bupropion 3IBD (Niu et al., 2011)		X													X
4-*tert*-butylphenylacetylene (BPA) 3IBD (Lin et al., 2011)		X					X	X			X				
Cyclophosphamide 3UA5 (Lautier et al., 2016)							X	X			X	X		X	X
2,3′,4,4',5-pentachlorobiphenyl (CB118)[d] 3IBD (Mise et al., 2016)			X									X			
Deschloroketamine 3IBD (Wang et al., 2019b)		X					X				X				X
Efavirenz 3IBD (Niu et al., 2011)		X										X			X
Fluoroketamine 3IBD (Wang et al., 2019b)		X					X				X				X
Garcinol 5UFG[d] (Bolla et al., 2021)	X	X		X	X	X		X	X	X					
Herbacetin[f] 5UDA (Qian et al., 2022)											X				X
Ketamine 3IBD (Wang et al., 2019b)		X					X				X				X
Mephobarbital 3IBD (Niu et al., 2011)			X									X			X
1,2,3,4,6,7,8,9-octachlorodibenzo-*p*-dioxin (OCDD) 3UA5 (Maldonado-Rojas et al., 2016)		X	X				X	X				X			X
2,2',3,4',5,5′,6-heptachlorobiphenyl (PCB-187) 3UA5 (Maldonado-Rojas et al., 2016)		X	X				X	X			X				X
Propofol 3IBD (Niu et al., 2011)		X									X				X
Propofol 2,6-di-*sec*-butyl phenol analog 3IBD (Niu et al., 2011)							X								X
Sauchinone 3IBD (Gong et al., 2018)		X					X	X							X
Ticlopidine 3IBD (Gay et al., 2010)		X					X				X	X			X
Ticlopidine 5UFG[d] (Bolla et al., 2021)		X	X		X		X[b]	X			X	X			X
Triclosan 3IBD (Zhang et al., 2021)							X				X				X
1-(4-hydroxy-3-methoxyphenyl)-5-(2-nitrophenyl)penta-1, 4-dien-3-1 (WZ35)[f] 5UDA (Wang et al., 2020a)														X	

TABLE 1 *continued*

Bound ligand PDB ID (reference)	Active site residues[a]															
	A298	G299	T300	E301	T302	L362	L363	G366	V367	P368	I370	D385	C475	V477	G478	K479
Amlodipine 3UA5 (Shah et al., 2012)	**X**	**X**	**X**	**X**	**X**		**X**	**X**	**X**	**X**			**X**	**X**	**X**	
4-benzylpyridine 3QOA (Shah et al., 2011)	**X**			**X**	**X**	**X**	**X**		**X**					**X**		
Bornane 5UDA (Shah et al., 2017)	**X**				**X**		**X**		**X**					**X**		
Bornyl bromide 5UAP (Shah et al., 2017)	**X**				**X**		**X**		**X**					**X**		
(+)-3-carene 4RRT (Shah et al., 2015)	**X**				**X**		**X**		**X**					**X**		
4-(4-chlorophenyl)imidazole 3IBD (Gay et al., 2010)	**X**				**X**		**X**		**X**					**X**		
Efavirenz 2-desoxo-2-methyl 5WBG (Shah et al., 2018)	**X**				**X**		**X**		**X**					**X**		
(-)-myrtenyl bromide 5UEC (Shah et al., 2017)	**X**				**X**		**X**		**X**					**X**		
(-)-myrtenyl bromide 5UFG[d] (Shah et al., 2017)	**X**				**X**		**X**		**X**					**X**		
4-(4-nitrobenzyl)pyridine 3QU8 (Shah et al., 2011)	**X**			**X**	**X**		**X**		**X**					**X**		
(+)-α-pinene 4I91 (Wilderman et al., 2013)	**X**				**X**		**X**		**X**					**X**		
(+)-α-pinene 4ZV8[c] (Liu et al., 2016)	**X**				**X**		**X**		**X**					**X**		
Sabinene 4RQL (Shah et al., 2015)	**X**				**X**		**X**		**X**					**X**		
2,2',4,4'-tetrabromodiphenyl ether (BDE-47) 3IBD (Zhang et al., 2021)	X				X		X		X	X						
BDE-47 3UA5 (Maldonado-Rojas et al., 2016)					X	X	X		X							
3-hydroxy-2,2′,4,4′-tetrabromodiphenyl ether (3-OH-BDE-47) 3UA5 (Maldonado-Rojas et al., 2016)				X	X	X	X		X							
5-hydroxy-2,2′,4,4′-tetrabromodiphenyl ether (5-OH-BDE-47) 3UA5 (Maldonado-Rojas et al., 2016)				X	X	X	X									
6-hydroxy-2,2′,4,4′-tetrabromodiphenyl ether (6-OH-BDE-47) 3UA5 (Maldonado-Rojas et al., 2016)	X				X	X	X		X							
2,2',4,4',5-pentabromodiphenyl ether (BDE-99) 3UA5 (Maldonado-Rojas et al., 2016)	X				X	X	X		X					X		
2,2',4,4',6-pentabromodiphenyl ether (BDE-100) 3UA5 (Maldonado-Rojas et al., 2016)	X				X	X	X		X					X		
3-hydroxy-2,2',4,4',6-pentabromodiphenyl ether (3-OH-BDE-100) 3UA5 (Maldonado-Rojas et al., 2016)	X				X	X	X		X							
3′-hydroxy-2,2',4,4',6-pentabromodiphenyl ether (3′-OH-BDE-100) 3UA5 (Maldonado-Rojas et al., 2016)	X			X	X	X	X		X							
5′-hydroxy-2,2',4,4',6-pentabromodiphenyl ether (5′-OH-BDE-100) 3UA5 (Maldonado-Rojas et al., 2016)	X				X	X	X		X					X		
6'-hydroxy-2,2',4,4',6-pentabromodiphenyl ether (6'-OH-BDE-100) 3UA5 (Maldonado-Rojas et al., 2016)	X				X	X	X		X					X		
Bromoketamine 3IBD (Wang et al., 2019b)	X				X		X		X					X		
Bupropion 3IBD (Niu et al., 2011)	X			X	X		X		X	X				X	X	
4-*tert*-butylphenylacetylene (BPA) 3IBD (Lin et al., 2011)	X			X	X									X		
Cyclophosphamide 3UA5 (Lautier et al., 2016)	X				X		X		X					X		
2,3′,4,4',5-pentachlorobiphenyl (CB118)[d] 3IBD (Mise et al., 2016)							X							X		
Deschloroketamine 3IBD (Wang et al., 2019b)	X				X		X		X					X		
Efavirenz 3IBD (Niu et al., 2011)	X			X	X		X		X					X	X	
Fluoroketamine 3IBD (Wang et al., 2019b)	X				X		X		X					X		
Garcinol 5UFG[d] (Bolla et al., 2021)											X	X				
Herbacetin[f] 5UDA (Qian et al., 2022)	X				X											X
Ketamine 3IBD (Wang et al., 2019b)	X				X		X		X					X		
Mephobarbital 3IBD (Niu et al., 2011)	X			X	X		X	X	X					X		X
1,2,3,4,6,7,8,9-octachlorodibenzo-*p*-dioxin (OCDD) 3UA5 (Maldonado-Rojas et al., 2016)	X				X	X	X		X					X		
2,2',3,4',5,5′,6-heptachlorobiphenyl (PCB-187) 3UA5 (Maldonado-Rojas et al., 2016)	X				X	X	X		X							
Propofol 3IBD (Niu et al., 2011)	X			X	X		X		X					X	X	
Propofol 2,6-di-*sec*-butyl phenol analog 3IBD (Niu et al., 2011)	X			X	X		X		X					X	X	X
Sauchinone 3IBD (Gong et al., 2018)	X			X	X		X	X	X	X				X		
Ticlopidine 3IBD (Gay et al., 2010)	X				X		X		X					X		
Ticlopidine 5UFG[d] (Bolla et al., 2021)	X					X	X		X					X		
Triclosan 3IBD (Zhang et al., 2021)	X			X	X		X		X						X	
1-(4-hydroxy-3-methoxyphenyl)-5-(2-nitrophenyl)penta-1, 4-dien-3-1 (WZ35)[f] 5UDA (Wang et al., 2020a)	X															

[a]Amino acids are numbered according to full-length refseq CYP2B6 (NX_P20813-1).
[b]The additionally mutated I114V CYP2B6 structure was used in these studies and position 114 was inconsistently observed to be within 5 Å of the ligands.
[c]This study used the additionally mutated Y244W CYP2B6 structure and W244 was not observed in the active site. Notably, this mutation did not change the amino acids within 5 Å of the ligand; therefore, we grouped both crystal structures (4I91 and 4ZV8) into the same row of this table.
[d]These entries reflect only the amino acids reported by the authors, although the existence of additional active site residues is likely.

TABLE 2

CYP2B6 active site mutations and their effects on metabolic kinetics

To our knowledge, this table reflects the only data available on CYP2B6 active site mutagenesis characterized via kinetic parameter measurement.

Substrate [metabolic method]		Active site mutations[b]															
		I114T	I114V	F206A	I209L	S294D	L363V	V367A	V367F	V367H	V367L	V367S	V367T	I370R	C475I	C475S	V477D
Androstenedione [16β-hydroxylation]	ΔK_m[d]	—	—	—	—	—	nr	—	—	—	—	—	—	—	—	—	—
	Δk_{cat}	—	—	—	—	—	↑↑↑	—	—	—	—	—	—	—	—	—	—
Bupropion [4-hydroxylation]	ΔK_m	↑↑↑	—	—	—	—	—	—	—	—	—	—	—	—	—	—	—
	Δk_{cat}	↓↓↓	—	—	—	—	—	—	—	—	—	—	—	—	—	—	—
7-butoxycoumarin [Variant oxidation]	ΔK_m	—	—	—	nr	nr	nr	—	—	—	nr	—	—	—	—	—	—
	Δk_{cat}	—	—	—	→	↓↓↓	↓↓↓	—	—	—	nc	—	—	—	—	—	—
Cyclophosphamide [4-hydroxylation]	ΔK_m	—	↓↓	—	—	—	—	—	↑↑	nr	↑	nr	↑	—	→	—	nr
	Δk_{cat}	—	↑	—	—	—	—	—	↓↓	↓↓↓	↑	↓↓↓	↓↓	—	↓↓↓	—	↓↓↓
Efavirenz [8-hydroxylation]	ΔK_m	↑↑↑	—	—	—	—	—	—	—	—	—	—	—	—	—	—	—
	Δk_{cat}	↓↓↓	—	—	—	—	—	—	—	—	—	—	—	—	—	—	—
3-cyclopentyloxy-*N*-(3,5-dichloro-4-pyridyl)-4-methoxybenzamide (RP 73401) [Cyclopentyl ring *trans*-hydroxylation]	ΔK_m	—	—	—	—	—	↑	—	—	—	—	—	—	nr	—	nr	—
	Δk_{cat}	—	—	—	—	—	→	—	—	—	—	—	—	→	—	→	—
4-trifluoromethyl-7-ethoxycoumarin (7-EFC) [*O*-deethylation]	ΔK_m	—	—	nc	↑↑↑	↑↑↑	nr /↓[e]	nc	—	—	→	—	—	nr	—	nr	—
	Δk_{cat}	—	—	→	→	↓↓↓	↑/[e]	↓↓	—	—	→	—	—	↑	—	→	—
							↓↓↓										

TABLE 2 *continued*

Substrate [metabolic method]	Active site mutations[b]														References
	V477E	V477F	V477I	V477T	V477W	V477Y	G478A	G478E	G478S	G478V	I114V/V477W	SRS 1[c]	SRS 5[c]	SRS 6[c]	
Androstenedione	—	—	—	—	—	—	—	—	—	—	—	nr	nr	nr	(Domanski et al., 1999)
[16β-hydroxylation]	—	—	—	—	—	—	—	—	—	—	—	nc	nc	↑↑↑	
Bupropion	—	—	—	—	—	—	—	—	—	—	—	—	—	—	(Radloff et al., 2013)
[4-hydroxylation]	—	—	—	—	—	—	—	—	—	—	—	—	—	—	
7-butoxycoumarin	—	nr	—	—	—	—	—	—	—	—	—	—	—	—	(Spatzenegger et al., 2003)
[Variant oxidation]	—	↑↑	—	—	—	—	—	—	—	—	—	—	—	—	
Cyclophosphamide	nr	↓	↓	↑	↓	↑	↑	nr	nr	↓	↓↓↓	—	—	—	(Nguyen et al., 2008)
[4-hydroxylation]	↓↓↓	↑	↑	↓	↑	↓↓	↓↓	↓↓↓	↓↓↓	↓	↓	—	—	—	
Efavirenz	—	—	—	—	—	—	—	—	—	—	—	—	—	—	(Radloff et al., 2013)
[8-hydroxylation]	—	—	—	—	—	—	—	—	—	—	—	—	—	—	
3-cyclopentyloxy-*N*-	—	—	nr	—	—	—	—	—	—	—	—	—	—	—	(Domanski et al., 1999)
(3,5-dichloro-4-pyridyl)-4-methoxybenzamide (RP 73401) [Cyclopentyl ring *trans*-hydroxylation]	—	—	↓↓	—	—	—	—	—	—	—	—	—	—	—	
4-trifluoromethyl-7-ethoxycoumarin (7-EFC)	—	↑	nr	—	—	—	—	—	—	—	—	nr	nr	nr	(Domanski et al., 1999; Spatzenegger et al., 2003; Lin et al., 2016)
[*O*-deethylation]	—	↑	↓	—	—	—	—	—	—	—	—	↓↓↓	↓↓↓	↑	

[b]Amino acids are numbered according to full-length refseq CYP2B6 (NX_P20813-1).
[c]These entries represent the mutations of SRS 1, 5, and 6 of CYP2B6 to the corresponding CYP2B1 sequences (Domanski et al., 1999).
[d]The directional changes tabulated here are relative to the CYP2B6 wild-type. One arrow indicates a change between 1-fold and twofold; two arrows indicate a change between twofold and threefold; three arrows indicate a change greater than threefold; "nc" indicates no notable change; "nr" indicates no reported value; em-dashes indicate unexplored kinetics.
[e]The observed effect on K_m and k_{cat} differed depending on the L363V CYP2B6 mutant being expressed in baculovirus-infected insect (Domanski et al., 1999)/*E. coli* JM109 cells (Spatzenegger et al., 2003).

TABLE 3

Expression system-dependence of kinetic parameters during the metabolism of select substrates by wild-type CYP2B6.[a]

	EXPRESSION SYSTEMS										
SUBSTRATE [METABOLIC METHOD]	Human B-lymphoblastoid cell microsomes	293FT cell microsomes	COS-1 cell microsomes	COS-7 cell microsomes	Supersomes	Baculovirus-infected insect cell microsomes	*Saccharomyces cerevisiae* W(R) cell microsomes	*Escherichia coli* Topp 3 cells	*Escherichia coli* C41 DE3 cells	*Escherichia coli* DH5α cells	*Escherichia coli* JM109 cells
Bupropion [4-hydroxylation]	K_m: 107.5 μM k_{cat}: NR[b] (Ekins and Wrighton, 1999)	—[c]	K_m: 87 μM k_{cat}: 7.9 min^{-1} (Radloff et al., 2013)	—	—	K_m: 65 μM[d] k_{cat}: 2.73 min^{-1} (Lang et al., 2004) K_m: 153 μM[d] k_{cat}: 2.46 min^{-1} (Klein et al., 2005)	—	K_m: 8.8 μM k_{cat}: 2.6 min^{-1} (Bumpus et al., 2005)	K_m: 95 μM k_{cat}: 6.8 min^{-1} (Zhang et al., 2011)	K_m: 0.5 μM k_{cat}: 47 min^{-1} (Lee et al., 2018)	—
Cyclophosphamide [4-hydroxylation]	—	—	—	—	K_m: 1,400 μM k_{cat}: 338 min^{-1} (Xie et al., 2003) K_m: 2,680 μM k_{cat}: 301 min^{-1} (Ariyoshi et al., 2011)	—	K_m: 4,900 μM k_{cat}: 62.5 min^{-1} (Nguyen et al., 2008) K_m: 4,030 μM k_{cat}: 36 min^{-1} (Lautier et al., 2016)	—	K_m: 3,600 μM k_{cat}: 75.4 min^{-1} (Raccor et al., 2012)	—	—
Efavirenz [8-hydroxylation]	—	K_m: 4.09 μM k_{cat}: 0.35 min^{-1} (Watanabe et al., 2018)	K_m: 2.07 μM k_{cat}: 1.1 min^{-1} (Radloff et al., 2013)	—	K_m: 12.40 μM k_{cat}: 5.20 min^{-1} (Ward et al., 2003) K_m: 9.0 μM k_{cat}: 1.4 min^{-1} (Ogburn et al., 2010) K_m: 7.70 μM k_{cat}: 9.06 min^{-1} (Ariyoshi et al., 2011) K_m: 0.45 μM k_{cat}: 1.0 min^{-1} (Cox and Bumpus, 2014) K_m: 3.6 μM k_{cat}: NR (Cox and Bumpus, 2016)	—	—	K_m: 14.3 μM k_{cat}: 4.3 min^{-1} (Bumpus et al., 2006) K_m: NR k_{cat}: 6.8 min^{-1} (Bumpus and Hollenberg, 2008)	K_m: 7.3 μM k_{cat}: 4.0 min^{-1} (Zhang et al., 2011)	—	—
4-trifluoromethyl-7-ethoxycoumarin (7-EFC) [*O*-deethylation]	K_m: 1.7 μM k_{cat}: NR (Ekins and Wrighton, 1999)	K_m: 7.58 μM k_{cat}: 2.11 min^{-1} (Watanabe et al., 2018)	K_m: 5.50 μM k_{cat}: 3.93 min^{-1} (Jinno et al., 2003)	K_m: 7.0 μM[e] k_{cat}: 21.1 min^{-1} (Watanabe et al., 2010)	—	K_m: NR k_{cat}: 3.74 min^{-1} (Domanski et al., 1999)	K_m: 3.5 μM k_{cat}: 17 min^{-1} (Lautier et al., 2016)	K_m: 30.4 μM k_{cat}: 3.0 min^{-1} (Kumar et al., 2007)	K_m: 4.8 μM k_{cat}: 1.2 min^{-1} (Zhang et al., 2011)	—	K_m: 8.5 μM k_{cat}: 14 min^{-1} (Spatzenegger et al., 2003)

[a]According to our literature search, this is only a sample of kinetic parameters differing for the same CYP2B6 isoform, substrate, and metabolic method within various expression systems. Expression system-dependence of CYP2B6 kinetics can also be observed for polymorphic and nonpolymorphic CYP2B6 mutants (Domanski et al., 1999; Spatzenegger et al., 2003; Gadel et al., 2013; Zanger and Klein, 2013; Calinski et al., 2015; Gadel et al., 2015; Imaishi and Goto, 2018; Wang et al., 2020b).
[b]"NR" indicates values that were not reported.
[c]Em-dashes indicate unexplored kinetics.
[d]While CYP2B6 expression and thus k_{cat} determination was more reliable within insect cell microsomes, the authors only reported K_m values via CYP2B6 bupropion hydroxylase activity from COS-1 cell expression.
[e]These values are the average of multiple replicate averages for CYP2B6.1 K_m and k_{cat} determination reported by the authors.

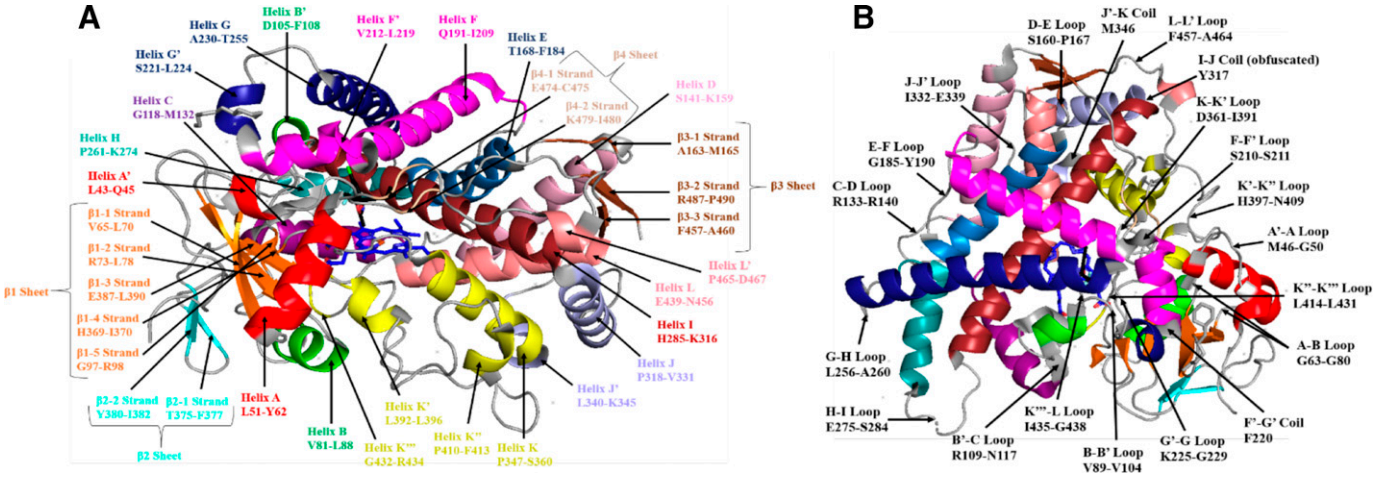

Fig. 1. A topological map of CYP2B6 structural elements. (A) The α-helix and *β*-strand/sheet topology (Nguyen et al., 2008) of crystallized CYP2B6 with a PDB identification code of 5WBG (Shah et al., 2018). The substrate (an efavirenz 2-desoxo-2-methyl analog) is colored in black while the heme group is colored in blue. Separate secondary structural elements are colored separately and named in matching colors. (B) The loop/coil topology (Zhao and Halpert, 2007; Nguyen et al., 2008) of crystallized CYP2B6 with a PDB identification code of 5WBG (Shah et al., 2018). α-helices and *β*-strands/sheets are colored as in (A). The orientation of CYP2B6 is rotated compared with (A) to maximize clarity in viewing loops and coils from one angle. While each discrete loop and coil are annotated herein, some commonly explored and larger topological features include helices, loops, and coils. For example, the F-G loop/cassette (Zhao and Halpert, 2007; Wilderman and Halpert, 2012) is composed of the F helix, F-F' loop, F' helix, F'-G' coil, G' helix, G'-G loop, and G helix, meaning that the F-G cassette consists of amino acids Q191-T255. The amino acids composing each structural element are numbered according to full-length refseq CYP2B6 (NX_P20813-1). All images were created in PyMOL.

be within 5 Å of bound ligands in CYP2B6 crystals include I101, V104, F108, I114, F115, F206, I209, S210, S294, F297, A298, G299, T300, E301, T302, L362, L363, G366, V367, P368, C475, V477, and G478 (Table 1), implicating the following CYP2B6 topological features in ligand binding/orientation: B-B' loop, Helix B', B'-C loop, Helix F, F-F' loop, Helix I, K-K' loop, *β*4-1 strand, and C-terminal coil (Fig. 1). Comparing CYP2B6 homology models and CYP2B6 crystal structures reveals a notable accuracy of the former (Supplemental Table 1 and Table 1) and underscores potential areas for future exploration. Based on homology models, Lewis and others have thoroughly predicted certain roles for amino acids observed to be in the putative CYP2B6 active site (Lewis and Lake, 1997; Domanski et al., 1999; Lewis, 1999; Lewis et al., 1999; Bathelt et al., 2002; Lewis et al., 2002; Wang and Halpert, 2002; Salonen et al., 2003; Spatzenegger et al., 2003; Lewis et al., 2004; Kent et al., 2006; Lewis et al., 2006; Nguyen et al., 2008; Lewis et al., 2010). Many of these amino acids, to our knowledge, have not been similarly characterized via more modern in silico techniques with known CYP2B6 crystal structures available (Table 1). Such efforts could yield intriguing insights into the CYP2B6 structure–function relationship.

Functions and Plasticity of CYP2B6 Active Site Residues. In consideration of the space limit, we henceforth focus this section on CYP2B6 crystal structures and CYP2B6 crystal-based molecular docking experiments. However, the aforementioned findings made by Lewis and others using CYP2B6 homology models are necessary to best comprehend our current understanding of the CYP2B6 structure–function relationship. Of the 23 active site amino acids observed in CYP2B6 crystals, 10 of them appear within 5 Å of the bound ligand in almost all of the existing structures (Table 1). These largely hydrophobic residues are I101, I114, F115, F206, F297, A298, T302, L363, V367, and V477. It has been found that I101 is involved in concerted movement with F115 and V477 to allow 4-CPI binding with the loss of V104 from the active site (Gay et al., 2010; Halpert, 2011). I101, V104, I209, and S210 flex away from the heme to allow the binding of larger ligands by CYP2B6, such as amlodipine (Shah et al., 2012). Another example of concerted residue movement is present within the CYP2B6-4-benzylpyridine (4-BP) and CYP2B6-amlodipine crystal structures as L362 protrudes further into the active site than previously identified while T302 reaches closer to the pyridine ring of 4-BP and the ethoxy oxygen of amlodipine (Shah et al., 2011; Shah et al., 2012). Similarly, the CYP2B6 crystal complexed with the efavirenz 2-desoxo-2-methyl analog showed that the cyclopropyl group of the analog resided between the side chains of F206 and T302 (Shah et al., 2018). On the other hand, the I101 and F115 side chains have the trifluoro group of efavirenz itself (Niu et al., 2011) and the efavirenz 2-desoxo-2-methyl analog oriented toward them (Shah et al., 2018). E301 and T302 contributed water-mediated hydrogen bonds to efavirenz along with the hydrophobic stabilization of it in the CYP2B6 active site by I101, F297, V367, and G478 (Niu et al., 2011; Radloff et al., 2013).

Molecular docking of propofol, the propofol 2,6-di-*sec*-butyl phenol analog, bupropion, and 4-*tert*-butylphenylacetylene (BPA) revealed strong interaction energies with I101, I114, F297, A298, L363, V367, and V477 forming hydrophobic contacts and E301 and/or T302 forming hydrogen bonds with the ligands (Lin et al., 2011; Niu et al., 2011; Radloff et al., 2013). The hydrophobicity of I101, I114, L363, V367, and V477 were also deemed important for favorable CYP2B6-mediated interactions with ketamine, bromoketamine, fluoroketamine, and deschloroketamine (Wang et al., 2019b). Generally, the hydrophobic residues within the putative CYP2B6 active site contribute greatly to the strong binding of polybrominated diphenyl ethers (PBDEs) and polychlorinated biphenyls (PCBs) such as 2,2',3,4',5,5',6-heptachlorobiphenyl (PCB-187) and 1,2,3,4,6,7,8,9-octachlorodibenzo-*p*-dioxin (OCDD) (Maldonado-Rojas et al., 2016). 2,3′,4,4',5-Pentachlorobiphenyl (CB118) is specifically stabilized within CYP2B6 through hydrophobic contacts of V104 and L363 with the 5′- and 2-positions of CB118, respectively (Mise et al., 2016). Molecular docking studies of herbal medicines such as sauchinone and garcinol have revealed similar contributions of the hydrophobic CYP2B6 active site residues to substrate binding (Gong et al., 2018; Bolla et al., 2021). Nearly all residues interacting with triclosan and 2,2',4,4'-tetrabromodiphenyl ether (BDE-47) are nonpolar as well (Zhang et al., 2021). An exception is that the carboxylate oxygen of A298 forms a hydrogen bond with the phenolic hydrogen of triclosan (Zhang et al., 2021). The three largely hydrophobic pockets predicted within the homology modeled CYP2B6 active

site (Bathelt et al., 2002) were visualized via CYP2B6 crystal-based molecular docking with cyclophosphamide (Lautier et al., 2016). The oxazaphosphorin ring of cyclophosphamide was surrounded by F206, A298, T302, and L363 (pocket A) with one chloroethyl side chain located near I114, F115, S294, and F297 (pocket B); the second chloroethyl side chain was bound by the roof of the binding cavity, composed of residues I209, V367, and V477 (pocket C) (Bathelt et al., 2002; Lautier et al., 2016).

The importance of hydrogen bonding for ligand binding/orientation should not be underestimated. S294 and A298 contributed hydrogen bonds to the molecularly docked 1-(4-hydroxy-3-methoxyphenyl)-5-(2-nitrophenyl)penta-1,4-dien-3-1 (WZ35) (Wang et al., 2020a). F297, A298, and K479 also mediate hydrogen bonds for the stabilization of herbacetin above the CYP2B6 heme (Qian et al., 2022). Mephobarbital is stabilized through hydrogen bonds from E301, T302, and K479 along with many of the hydrophobic contacts already discussed (Niu et al., 2011). E301 exhibits an interesting behavior within the CYP2B6 crystal complexed with 4-CPI as it flexes out of the active site to hydrogen bond with a nearby water molecule rather than the ligand, although this allows 4-CPI to interact hydrophobically with F206 (Gay et al., 2010). This same phenomenon is observed for crystallized CYP2B6 complexed with 4-BP and 4-(4-nitrobenzyl)pyridine (4-NBP) where E301 interacts directly with Q172 and indirectly with S304 in a P450 subfamily 2B-conserved hydrogen bond network stabilizing the E and I helices (Shah et al., 2011). However, the side chain of E301 protrudes into the cavity where 4-CPI would be in the CYP2B6-amlodipine crystal to interact with T305 and R308 (Shah et al., 2012; Chen et al., 2018). The plasticity of E301 is further noted through molecular docking as bupropion induces its movement to the edge of the CYP2B6 active site, which is more centralized within when propofol and efavirenz are docked (Niu et al., 2011). E301 also forms a hydrogen bond with the CYP2B6 covalent modification site, T302, that is broken upon covalent binding of BPA to cause deleterious effects on active site conformation, plasticity, and catalysis (Lin et al., 2011; Watanabe et al., 2018).

Many compounds are stabilized within CYP2B6 by a combination of forces such as hydrogen bonding between E301 and PBDEs in addition to hydrophobic interactions between L363 and compounds like 2,2',4,4',5-pentabromodiphenyl ether (BDE-99), PCB-187, and OCDD (Maldonado-Rojas et al., 2016). L363 has long been defined as a residue critical for the CYP2B6 structure–function relationship with its further creation of hydrophobic contacts with 3-cyclopentyloxy-*N*-(3,5-dichloro-4-pyridyl)-4-methoxybenzamide (RP 73401 or Piclamilast), 7-butoxycoumarin, the terminal methyl of the 7-ethoxy group of 4-trifluoromethyl-7-ethoxycoumarin (7-EFC), and the N-methyl group of diazepam (Domanski et al., 1999; Lewis et al., 1999; Domanski and Halpert, 2001; Spatzenegger et al., 2003; Niu et al., 2011; Wang et al., 2019b). However, L363 was found to be confoundingly insignificant compared with other residues in the binding of 4-CPI, efavirenz, propofol, and the propofol 2,6-di-*sec*-butyl phenol analog (Gay et al., 2010; Niu et al., 2011). Relative to other hydrophobic CYP2B6 active site residues, L363 and V477 weakly interact with efavirenz and the benzyl groups of propofol and the propofol 2,6-di-*sec*-butyl phenol analog, which differs from their strong hydrophobic interactions with bupropion and mephobarbital (Niu et al., 2011). The local hydrophobicity and flexibility of V477 in the CYP2B6 active site nonetheless affects the metabolism of many of the same substrates that L363 is pertinent for such as RP 73401 and 7-butoxycoumarin (Domanski et al., 1999; Spatzenegger et al., 2003; Gay et al., 2010; Shah et al., 2012). Like many phenylalanine residues, L363 and T302 have also been implicated in conjugated π systems upon binding sauchinone and herbacetin, respectively (Gong et al., 2018; Qian et al., 2022).

Phenylalanine residues in the putative CYP2B6 active site are uniquely involved in hydrophobic interactions, π-π stacking, *and* halogen-π interactions. The bulky F108, F115, F206, F292, and F297 residues were found to be most involved in individual small movements culminating into large changes in the CYP2B6 active site volume, which ranges from 279 $Å^3$ to 755 $Å^3$ depending on the bound ligand (Halpert, 2011; Shah et al., 2011; Shah et al., 2012; Jang et al., 2014). F108 and F115 exhibit concerted movement in the binding of 4-CPI such that F108 shifts toward the G helix to accommodate the flexion of F115 out of the CYP2B6 active site (Gay et al., 2010). F108 is a residue not usually within 5 Å of CYP2B6 ligands, but the nitro moiety of 4-NBP points directly toward it and forces its accommodating flexion (Shah et al., 2011). Without the nitro moiety, the benzyl group of 4-BP points toward F115 instead (Shah et al., 2011). F108 also forms an important bromine-π bond for the stabilization of bornyl bromide in the CYP2B6 active site (Shah et al., 2017). (-)-Myrtenyl bromide was crystallized in a wild-type CYP2B6 active site and formed a bromine-π bond with F297; (-)-myrtenyl bromide was also crystallized in an I114V mutant CYP2B6 active site, allowing it to form bromine-π bonds with F108, F115, and F297 (Shah et al., 2017). The efavirenz 2-desoxo-2-methyl analog crystallized within CYP2B6 was found to form a chlorine-π bond with F108 that was allowed by a corresponding flexion of F206 and F297 to expand the active site volume (Shah et al., 2018). F206 also moves to occupy the space created by the flexion of E301 in the CYP2B6-4-CPI crystal while entering the active sites of the CYP2B6-4-BP and CYP2B6-4-NBP crystals as F297 rotates out (Gay et al., 2010; Halpert, 2011; Shah et al., 2011). The same concerted movement of F206 and F297 occurs to a more exaggerated extent to shrink the active site around (+)-α-pinene (Wilderman et al., 2013).

It has been hypothesized that there are two binding modes within the CYP2B6 active site, termed "A" and "B"; the former is more common and characterized by F206 moving into and F297 moving out of the active site while the latter involves the inverse action (Shah et al., 2015). Regardless, π-π stacking between F206 and selegiline along with herbacetin has also been predicted to be important for their binding/orientation/metabolism (Salonen et al., 2003; Qian et al., 2022). F297 similarly mediates π-π stacking with the benzyl groups of propofol, the propofol 2,6-di-*sec*-butyl phenol analog, and mephobarbital (Niu et al., 2011). F206 forms a sort of π stacking interaction with the -NH group of amlodipine's pyridine moiety while F297 forms a chlorine-π bond with the chlorophenyl moiety of 4-CPI to stabilize these ligands (Shah et al., 2015). F297 was deemed exceptionally important for facilitating π-π stacking with ketamine, bromoketamine, fluoroketamine, and deschloroketamine (Wang et al., 2019b). Phenylalanine residues are also capable of forming hydrogen bonds with ligands, as seen between F297, the propofol 2,6-di-*sec*-butyl phenol analog, and herbacetin (Niu et al., 2011; Qian et al., 2022). The F-G cassette (Fig. 1) contains many phenylalanine residues and forms the "active site roof" in ligand-bound structures, is embedded within the lipid bilayer in ligand-unbound structures, and is thought of as the most plastic region of P450 subfamily 2B isoforms (Halpert, 2011; Wilderman and Halpert, 2012; Li et al., 2020). The hydrophobic F-G cassette helps create a lipophilic polarization within the CYP2B6 active site such that larger hydrophobic and smaller hydrophilic pockets contribute to substrate specificity; the identity of residues within those pockets delineate the form of chemical contribution (e.g., hydrogen bonding, hydrophobic interactions, π-π stacking) while also sterically contributing to such specificity (Mise et al., 2016).

In Silico Challenges with CYP2B6. In silico methods may be useful for explaining in vitro results, but they are not always 100% accurate on their own (Salonen et al., 2003; Radloff et al., 2013; Dmitriev et al., 2021) as some favorable ligand binding events visualized with X-ray crystallography or molecular docking can be unproductive in vitro (Talakad et al., 2011; Kobayashi et al., 2014; Maldonado-Rojas et al.,

2016). A complete in silico characterization of the CYP2B6 structure–function relationship is limited due to many variables influencing the CYP2B6-ligand binding/metabolism event (de Graaf et al., 2005). For example, CYP2B6 has been shown to have no regiospecificity for triclosan monohydroxylation (Zhang et al., 2021), catalyze testosterone 16α- and 16*β*-hydroxylation (Ekins and Wrighton, 1999), and strictly perform efavirenz 8-hydroxylation (Ward et al., 2003). While computerized methods are quicker/cheaper than in vitro methods for the pharmacological screening of new chemical entities, the measuring of in vitro catalytic data remains necessary to establish their full metabolic profile. The in vitro data providing insights into the structure–function relationship of the CYP2B6 active site will be reviewed next.

In Vitro Insights

CYP2B6 Substrate, Stereo-, and Regiospecificity. Recent work has been dedicated to understanding two important considerations for CYP2B6 substrate specificity: the substrate stereochemistry (Roy et al., 1999; Totah et al., 2007; Wang et al., 2018; Wang et al., 2019a) and, as detailed in the previous section, the various moieties composing the substrate (Ekins et al., 2008; Lewis et al., 2010; Cox and Bumpus, 2014; Cox and Bumpus, 2016; Liu et al., 2016; Wang et al., 2019b). Generally, CYP2B6 has a lower K_m for the *(S)*-enantiomers but a higher k_{cat} for the *(R)*-enantiomers of substrates (Niwa et al., 2011). CYP2B6 and CYP3A4 also tend to differ in their enantioselectivity as seen with ifosfamide since the former preferentially metabolizes *(S)*-ifosfamide while the latter prefers *(R)*-ifosfamide (Roy et al., 1999; Niwa et al., 2011). Some have attributed this observation to the potential for an enantiomeric/mirror arrangement of the CYP2B6 and CYP3A4 active sites (Lu et al., 2006). *(S)*-methadone has a lower K_m for *N*-demethylation by CYP2B6, which is also the principal metabolizer of racemic methadone (Gerber et al., 2004; Crettol et al., 2005; Zanger et al., 2007; Totah et al., 2008). CYP2B6 preferentially hydroxylates *(S)*-bupropion to *(S,S)*-hydroxybupropion (Coles and Kharasch, 2008; Sager et al., 2016; Wang et al., 2020b) and is solely responsible for the *N*-demethylation of *(S)*-mephobarbital (Kobayashi et al., 1999; Wang and Tompkins, 2008). An intriguing feature of CYP2B6-mediated bupropion metabolism is the selective formation of *(R,R)*- and *(S,S)*-hydroxybupropion but neither *(R,S)*- nor *(S,R)*-hydroxybupropion when using *(R)*- and *(S)*-bupropion as substrates, respectively (Coles and Kharasch, 2008; Bamfo et al., 2022). Explanations for these observations remain elusive but may manifest with deeper exploration of the structure–function relationship of the CYP2B6 active site. Contrary to its general *(S)*-enantioselectivity, CYP2B6 had a 77% lower K_m value for *(R)*-citalopram than *(S)*-citalopram (Niwa et al., 2011). The CYP2B6 K_m values for *(R)*-fluoxetine (Niwa et al., 2011), *(S)*-ketamine (Niwa et al., 2011; Wang et al., 2018), *(R)*-norketamine (Desta et al., 2012), and *(S)*-nicotine (Bloom et al., 2019) were all lower than their opposite enantiomers. The enantioselectivity of CYP2B6 for *(S)*-efavirenz was found to be the greatest with a higher active site affinity and 10-fold greater k_{cat} than *(R)*-efavirenz (Wang et al., 2019a).

The k_{cat} values are larger for *(S)*-ifosfamide 4-hydroxylation (Roy et al., 1999; Niwa et al., 2011), *(R)*-methadone *N*-demethylation (Gerber et al., 2004; Gadel et al., 2015), *(S)*-bupropion 4-hydroxylation (Coles and Kharasch, 2008; Wang et al., 2020b), and *(S)*-fluoxetine *N*-demethylation (Niwa et al., 2011) than their opposite enantiomers. The k_{cat} values for ketamine (Niwa et al., 2011; Li et al., 2013) and norketamine (Desta et al., 2012) are approximately equivalent between the *(R)*- and *(S)*-enantiomers. The k_{cat} in a recent CYP2B6-ketamine stereospecificity study, however, was higher for *(S)*-ketamine (Wang et al., 2018). This selection of example substrates seems to contradict the generalization made by Niwa et al. regarding K_m and k_{cat}, but there are confounding variations in kinetic parameters for the metabolism of the same substrates by CYP2B6 in the same or different expression systems (Table 3). For example, a lower CYP2B6 K_m for *(S)*-ketamine was found in an insect cell expression system but not within COS-1 cells (Li et al., 2013). The issue of lacking continuity in CYP2B6 kinetic parameters based on the expression system will be discussed further later. Beyond enantioselectivity, there are various moieties of substrates that seem to specifically promote CYP2B6-mediated metabolism (Cox and Bumpus, 2014; Wang et al., 2019b). Interesting observations have been made in this regard but remain unexplained from the perspective of the CYP2B6 structure–function relationship. For example, deuterating ifosfamide on its alpha and alpha' carbons reduced its K_m for CYP2B6 by over 50% (Calinski et al., 2015). Previous work has also tested the CYP2B6 structure–function relationship through novel modulations in the efavirenz chemical scaffold (Cox and Bumpus, 2014; Cox and Bumpus, 2016).

Most notably, efavirenz analogs lacking an intact oxazinone ring were not readily oxidized by CYP2B6 (Cox and Bumpus, 2014). The benzoxazine analog had an increased catalytic efficiency, revealing the efavirenz carbonyl group to abrogate CYP2B6-mediated metabolism due to possible steric clashes with L363 and V367 (Niu et al., 2011; Cox and Bumpus, 2016) or overstabilization in the active site via hydrogen bonds donated from E301 and T302 (Cox and Bumpus, 2014). Opening the cyclopropyl group increased K_m by over twofold as the greater rotational degrees of freedom may cause steric clashes (Cox and Bumpus, 2014). Efavirenz analogs with intact oxazinone rings and heteroatom substitutions remained as CYP2B6 substrates but had altered K_m values (Cox and Bumpus, 2016). Replacing the carbonyl with a methyl group increased the affinity for the CYP2B6 active site by over twofold, corroborating previous findings (Cox and Bumpus, 2014; Cox and Bumpus, 2016). An angularly projected methyl group off the oxazinone ring could avoid steric clashes and form favorable hydrophobic interactions with L363 and V367 (Cox and Bumpus, 2016). However, replacing the hydrogen bond-accepting ether of efavirenz with a secondary amine or saturated carbon increased the CYP2B6 K_m by over threefold (Cox and Bumpus, 2016). Liu et al. performed a similar study with 4-substituted-7-alkoxycoumarin derivatives where 7-EFC displayed the highest catalytic efficiency (Liu et al., 2016). Increasing the 7-alkoxy chain length from an ethyl to a propyl and butyl group caused a proportional decrease in CYP2B6 K_m and k_{cat} (Liu et al., 2016). A similar decrease occurred when increasing the bulk of 7-ethoxycoumarin derivatives by placing a methyl group at position 4, but turnover was increased when that bulky 4-substituent was halogenated (Liu et al., 2016). The identity of substrate halogen atoms generally increases affinity for CYP2B6 such that dibromo > dichloro for phenoxyaniline (POA) analogs (Chen et al., 2018) and Br > Cl > F for ketamine analogs (Wang et al., 2019b). The effect of halogenating CYP2B6 substrates is substrate-dependent but generally promotes high CYP2B6 binding affinity by increasing substrate hydrophobicity (Chen et al., 2018; Wang et al., 2019b).

As aforementioned, the regiospecificity of CYP2B6 can obfuscate its structure–function relationship by being strict or unspecified depending on the substrate. Uniquely, CYP2B6 can mediate the *O*-demethylation and *ortho*-hydroxylation of methoxychlor (Hodgson and Rose, 2007; Wang and Tompkins, 2008). PBDEs such as BDE-47 can also form up to nine different metabolites when oxidized by CYP2B6 (Erratico et al., 2015). The K_m and k_{cat} values were very similar for the CYP2B6-mediated formation of 4'-hydroxy-2,2',4,5′-tetrabromodiphenyl ether (4'-OH-BDE-49), 5-hydroxy-2,2',4,4'-tetrabromodiphenyl ether (5-OH-BDE-47), and 6-hydroxy-2,2',4,4'-tetrabromodiphenyl ether (6-OH-BDE-47), implying that CYP2B6 showed no preference for *ortho*-, *meta*-, or *para*-hydroxylation (Erratico et al., 2015). Interestingly, 2,2',4,4',6-pentabromodiphenyl ether (BDE-100) differs from the BDE-47 structure only by a third *ortho*-

substituted bromine atom, which significantly lowers its ability to be metabolized by CYP2B6 (Gross et al., 2015). The variety of metabolites formed from CYP2B6-mediated BDE-47 metabolism suggests that it can bind within the active site in a variety of metabolically active orientations (Erratico et al., 2015). CB118 must also either bind with positional variance within the CYP2B6 active site or its single binding mode places its carbons 3 and 5 in close enough proximity to the heme for monooxygenation (Mise et al., 2016). The former case is probably more likely considering efavirenz hydroxylation on carbons 7 and 8 but the strict 8-hydroxyefavirenz formation by CYP2B6 (Ward et al., 2003) and 7-hydroxyefavirenz formation by CYP2A6 (Ogburn et al., 2010). CYP2B6-mediated metabolism of 8-hydroxyefavirenz to 7,8-dihydroxyefavirenz and 8,14-dihydroxyefavirenz has also been observed, further exemplifying the existence of more than one productive binding mode and flexible regiospecificity (Avery et al., 2013). Without any further research into the structure–function relationships between CYP2B6 and these substrates, it is difficult to identify the reason for these observations.

Site-directed mutagenesis of CYP2B6 followed by metabolic characterization with various substrates is the "gold-standard" for elucidating in vitro insights into the structure–function relationship. Common substrates that have been used in these efforts include bupropion (Lang et al., 2004; Klein et al., 2005; Radloff et al., 2013; Wang et al., 2020b), cyclophosphamide (Nguyen et al., 2008; Ariyoshi et al., 2011; Raccor et al., 2012), 7-EFC (Domanski et al., 1999; Jinno et al., 2003; Spatzenegger et al., 2003; Kumar et al., 2007; Liu et al., 2016; Watanabe et al., 2018), efavirenz (Bumpus et al., 2006; Zhang et al., 2011; Watanabe et al., 2018; Wang et al., 2019a), and ketamine (Li et al., 2013; Wang et al., 2018) among others. Bupropion 4-hydroxylation (Desta et al., 2007) and *(S)*-efavirenz 8-hydroxylation (Wang et al., 2019a) are excellent probes for CYP2B6 activity in complex expression systems like human liver microsomes as such reactions are catalyzed nearly exclusively by CYP2B6. Although they are not clinical pharmaceuticals, monoterpenes have also been suggested as ideal in vitro CYP2B6 active site probes (Wang et al., 2019b). There are several CYP2B6 substrates that, to our knowledge, have not been kinetically parameterized with CYP2B6 mutants (Supplemental Table 2). The only substrates that have been used to kinetically characterize CYP2B6 active site mutants are androstenedione, bupropion, 7-butoxycoumarin, cyclophosphamide, efavirenz, RP 73401, and 7-EFC (Table 2).

Functionality of CYP2B6 Active Site Mutants. Substantial mutagenesis research has been done on clinically relevant CYP2B6 polymorphs, which are largely outside the active site and have been extensively reviewed by others (Zanger et al., 2007; Wang and Tompkins, 2008; Mo et al., 2009; Turpeinen and Zanger, 2012; Zanger and Klein, 2013; Naidoo et al., 2014; Langmia et al., 2021). A thorough summary of structure–function findings with CYP2B6 polymorphs outside of the active site is deserving of an independent review due to the large number of variants, and thus we will not explore them here. The sparse number of publications investigating the CYP2B6 active site through in vitro structure–function studies within the last 6 years (Table 2) reveals the potential to reignite such interests within our field. Originally, L363 within the K-K' loop of CYP2B6 (Fig. 1) was of particular interest as it is a unique residue compared with other P450 family 2 enzymes that have valine at that position (Domanski et al., 1999; Spatzenegger et al., 2003). An L363V mutation within CYP2B6 was found to increase the k_{cat} for androstenedione 16β-hydroxylation (Domanski et al., 1999) but decreased the k_{cat} for 7-butoxycoumarin oxidation (Spatzenegger et al., 2003) and the catalytic efficiency for RP 73401 hydroxylation (Domanski et al., 1999). More rigid and planar substrates like androstenedione may favor the larger active site volume that V363 allows. L363V had no significant effect on the k_{cat} of 7-EFC *O*-deethylation in baculovirus-infected insect cells (Domanski et al., 1999) yet decreased that catalytic efficiency in E. coli (Spatzenegger et al., 2003). Nonetheless, L363 in addition to F107 of the CYP2B6 B' helix (Fig. 1) were implicated in substrate-specific pertinence for RP 73401 metabolism (Domanski et al., 1999) while L363 also conferred a higher binding affinity for POA congeners that was decreased with a V363 substitution (Chen et al., 2018). There may be something necessary in the bulkier presence of F107 and L363 for allowing binding and oxidative metabolism of larger substrates with more rotational degrees of freedom like RP 73401 and 7-butoxycoumarin. F107 seems to possess substrate-specific importance as its mutation to valine or isoleucine had no significant effect on the catalytic efficiency of cyclophosphamide 4-hydroxylation (Nguyen et al., 2008) and 7-EFC *O*-deethylation (Domanski et al., 1999), respectively.

Single amino acid changes have even been shown to augment the cooperativity of CYP2B6 catalysis with L363V showing positive cooperativity and V367L showing negative cooperativity upon 7-EFC metabolism (Spatzenegger et al., 2003). A V367L single mutation within the K-K' loop of CYP2B6 (Fig. 1) also caused an elevated k_{cat} for cyclophosphamide 4-hydroxylation, which was an observation that was not made for the V367F/S/T/H mutations (Nguyen et al., 2008) nor when V367L CYP2B6 had 7-EFC or 7-butoxycoumarin as substrates (Spatzenegger et al., 2003). It is notable, though, that a V367A mutation decreased the k_{cat} for 7-EFC *O*-deethylation (Lin et al., 2016). V367 thereby affects CYP2B6-mediated metabolism on a substrate-specific basis with some substrates favoring a larger hydrophobic residue while others favor a smaller hydrophobic residue at position 367. Although CYP2B6.1 natively prefers 16β-hydroxylation of testosterone and androstenedione, placing the less bulky alanine within the F helix and K-K' loop at positions 206 and 367, respectively (Fig. 1), seems to increase the enzymatic preference for 16α-hydroxylation, which may be due to D-ring reorientation upon substrate binding that forces the 16α-carbon closer to the heme iron (Lin et al., 2016). The only polymorphic residue within the CYP2B6 active site belongs to the CYP2B6.35 haplotype, which had no catalytic activity with 7-EFC and efavirenz as substrates (Watanabe et al., 2018). This may be attributed to the deleterious presence of apoenzyme and location of G110V and I114T in SRS 1 (Gotoh, 1992; Watanabe et al., 2018); however, the other polymorphisms included within the CYP2B6.35 haplotype (E148D, M198T, and A279P) could also be responsible for the observed lack of enzymatic activity (Honda et al., 2011; Radloff et al., 2013; Watanabe et al., 2018; Desta et al., 2021). An I114T single mutant also displayed a remarkably reduced catalytic efficiency with bupropion and efavirenz as substrates (Radloff et al., 2013), suggesting that the small size of G110 and the hydrophobicity of I114 promotes wild-type levels of CYP2B6 catalysis.

Singularly testing CYP2B6 mutants from complex haplotypes is useful for determining the functional effects of discrete changes to CYP2B6, as was done for I114T despite its presence within CYP2B6.35 (Radloff et al., 2013). However, multiple mutations within one CYP2B6 isoform can have interactive effects on catalysis. The I114V/V477W CYP2B6 mutant remarkably enhanced the catalytic efficiency of cyclophosphamide 4-hydroxylation (Nguyen et al., 2008). The I114V substitution in the B'-C loop (Fig. 1) independently decreased the K_m of this reaction, perhaps by increasing accessibility for cyclophosphamide through the previously identified substrate access channel 2 (Cojocaru et al., 2007; Nguyen et al., 2008; Shah et al., 2012; Jang et al., 2014; Lautier et al., 2016), while the V477I, V477F, and V477W substitutions with expanding size and hydrophobicity increased the catalytic efficiency in that order (Nguyen et al., 2008). Altering position 477 to have polarity with V477S/T/Y/N/D/E mutations largely decreased cyclophosphamide metabolism (Nguyen et al., 2008). Another study has also suggested that replacing V477 with a larger hydrophobic residue like

phenylalanine may encourage a more catalytically active orientation of 7-EFC, 7-ethoxycoumarin, and 7-butoxycoumarin in the CYP2B6 active site (Spatzenegger et al., 2003). Further substantiating the substrate specificity of active site residue importance, wild-type V477 is apparently beneficial for the cyclopentyl ring *trans*-hydroxylation of RP 73401 (Domanski et al., 1999). Mutagenesis within CYP2B6 SRSs also
displays substrate specificity as discretely mutating CYP2B6 SRS 1 and 5 to the corresponding CYP2B1 sequences maintained wild-type levels of androstenedione 16β-hydroxylation but diminished 7-EFC *O*-deethylation (Domanski et al., 1999). The same was done for CYP2B6 SRS 2 and 6 where the former decreased the k_{cat} while the latter increased the k_{cat} with androstenedione and 7-EFC as substrates (Domanski et al., 1999).

The hydrophobicity of position 478 is also important for wild-type CYP2B6 activity as G478S and G478E single mutants were essentially inactive with cyclophosphamide as a substrate (Nguyen et al., 2008). Interestingly, a G478V single mutant had a similar catalytic efficiency to the wild-type for cyclophosphamide 4-hydroxylation while G478A significantly decreased that catalytic efficiency (Nguyen et al., 2008). Position 478 may require a hydrophobic residue that is either small (like glycine) or bulkier (like valine) for normal CYP2B6 functionality. The moderate bulk of A478 could potentially allow unfavorable steric clashes to occur within its seemingly hydrophobic pocket. Maintaining I209 and S294 as active site residues within the F helix and I helix, respectively (Fig. 1), is also necessary as the I209L and S294D CYP2B6 single mutants significantly diminished the k_{cat} with 7-butoxycoumarin and 7-EFC as substrates (Spatzenegger et al., 2003). In this case, the steric positioning of I209 appears advantageous to the CYP2B6 active site, and its mere isomerization is deleterious, even though the opposite was true with the L313I mutation (Watanabe et al., 2018). The localized polarity/hydrogen bonding capacity created by S294 near the heme may be important for CYP2B6-substrate interactions and/or topological interactions within CYP2B6. Furthermore, L199M increased, S207A did not affect, and K236N decreased, the CYP2B6 catalytic efficiency with cyclophosphamide as a substrate (Nguyen et al., 2008), which may be due to the localization of these residues in the F helix and G helix (Fig. 1), causing intricate modulations in the coordinated plasticity of the F-G cassette. An F206A mutation within CYP2B6 resulted in a slight decrease in k_{cat} with 7-EFC (Lin et al., 2016), suggesting that both the hydrophobicity and bulk at position 206 may be important for substrate binding/metabolism similar to the wild-type.

M365I and C475I CYP2B6 single mutants within the K-K' loop and β4-1 strand, respectively (Fig. 1), notably decreased k_{cat} with cyclophosphamide (Nguyen et al., 2008) but not when M365I and C475S had RP 73401 and 7-EFC as substrates (Domanski et al., 1999). Even though methionine and isoleucine have a comparable capacity for steric clashes, the effect of amino acid chemistry at position 365 is apparently substrate-specific. The nucleophilic nature of residue 475 seems important for CYP2B6-mediated catalysis, and the functionality of C475S makes it clear that there is no disulfide bridge formed by C475 that is pertinent for the structural/catalytic integrity of CYP2B6. Furthermore, M103V, R109K, N291S, and T292L CYP2B6 single mutants decreased the k_{cat} for RP 73401 and 7-EFC oxidation, but the S284H, N289M, T292A, and I370R mutations had less significant effects on k_{cat} (Domanski et al., 1999). It is interesting to consider T292 in the I helix of CYP2B6 (Fig. 1) and, therefore, its proximity to the active site. The preservation of CYP2B6 catalytic activity with the nonconservative T292A mutation versus the loss of function with the bulkier yet still hydrophobic leucine at position 292 suggests a unique and unpredictable mutational sensitivity within the I helix. Such speculation is corroborated by the aforementioned effects of the S294D and L313I mutations (Spatzenegger et al., 2003; Watanabe et al., 2018). The apparent sensitivity and elusiveness of the CYP2B6 structure–function relationship can be explained as a challenging product of its relatively uncharacterized active site (Table 2) and rampant expression system dependence of kinetic parameters (Table 3).

In Vitro Challenges with CYP2B6. The prominent in vitro challenges of substrate-dependent and expression system-dependent changes in catalysis remain unsolved (Domanski et al., 1999; Jinno et al., 2003; Bumpus et al., 2005; Klein et al., 2005; Wang et al., 2006; Zhao and Halpert, 2007; Wang and Tompkins, 2008; Honda et al., 2011; Zhang et al., 2011; Gadel et al., 2013). The former problem is expected and by nature connected with a thorough understanding of the CYP2B6 structure–function relationship, but the latter problem may obscure such an understanding. Though many kinetic data are compared internally within a single study, compiling these data and comparing across studies/expression systems reveals distinct inconsistencies that challenge the elucidation of the CYP2B6 structure–function relationship (Table 3). This is especially apparent when the kinetic parameters of K_m and k_{cat} should theoretically be constants for identical enzymatic isoforms catalyzing the same reactions on the same substrates. Therefore, it may be that the significant challenge of detailing the structure–function relationship of CYP2B6 is related to the discontinuity of catalytic data between the same isoforms with the same substrates in expression systems that are as different as 293FT cell microsomes (Watanabe et al., 2018) and E. coli (Zhang et al., 2011), as similar as COS-1 (Jinno et al., 2003) and COS-7 cell microsomes (Watanabe et al., 2010) or even identical (Gerber et al., 2004; Gadel et al., 2015). It is likely that standardizing in vitro experimental conditions for heterologous expression of CYP2B6.1 and its mutants when determining their kinetic parameters would provide the necessary framework for cross-study comparisons. It may be possible to optimize the CYP2B6 expression system, P450 oxidoreductase (POR):P450 ratio (El-Serafi et al., 2015; Wang et al., 2018; Wang et al., 2020b), and presence/absence/concentration of cytochrome b5 (cyt b5) (Shebley and Hollenberg, 2007; Bumpus and Hollenberg, 2008; Calinski et al., 2015; Yoo et al., 2019) for accessibility, affordability, and, most importantly, experimental accuracy and precision for laboratories in the field to use.

As the electron transferring redox partners of P450s that may have polymorph- and expression system-dependent levels of expression/activity, POR and cyt b5 can influence CYP2B6 substrate binding/metabolism in a complex and relatively unpredictable fashion (El-Serafi et al., 2015; Chen et al., 2018; Yoo et al., 2019). Moreover, the impact of membrane interactions involving the N-terminal domain of CYP2B6 on active site architecture also remains unknown. Until the heterologous expression of CYP2B6 is better optimized for cross-study comparisons, kinetic parameters, and structure–function findings elucidated from studies employing the heterologous expression of CYP2B6, particularly N-terminally truncated CYP2B6, should be interpreted with caution. Other enigmatic themes controverting common biochemical intuition are abundant within the CYP2B6 structure–function relationship. CYP2B6 has often been compared with CYP2B1 in an effort to extrapolate conclusions about the former enzyme's elusive behavior, but these reports should be handled carefully as their metabolic profiles are not always identical (Bumpus et al., 2005; Wang and Tompkins, 2008; Lin et al., 2016). Moreover, whole SRS mutations cannot necessarily confer the substrate specificity of CYP2B1 to CYP2B6 (Domanski et al., 1999), and the same is true for single residue mutations with F477V CYP2E1 obtaining CYP2B6-like activity with 7-EFC but V477F CYP2B6 not gaining activity with the CYP2E1-specific substrate, *p*-nitrophenol (Spatzenegger et al., 2003). CYP2B6 structure–function investigators have hypothesized that mutagenesis within active site residues is only useful for augmenting the function of certain P450 isoforms to behave more like other P450 isoforms if the substrates they natively metabolize are very similar (Spatzenegger

et al., 2003; Zhao and Halpert, 2007). Otherwise, changes in the highly conserved P450 backbone are necessary to alter the productive metabolism of substrates in a directed fashion (Spatzenegger et al., 2003; Zhao and Halpert, 2007; Fasan et al., 2019). The malleable CYP2B6 active site mold may be limited in its ability to metabolize various substrates of other P450s by the upper limits of its backbone flexibility. CYP2B6 was aptly dubbed an unusual P450 isoform due to the inexplicable preclusion of generalizations about catalytic consequences upon its mutagenesis (Wang et al., 2020b). However, what may seem inexplicable now may still be explained in the future.

Fertile Grounds for Future Insights

The ongoing optimization of current and advent of new in silico technologies will undoubtedly continue bolstering the accuracy of protein structure–function predictions. As such, new CYP2B6 crystals must continue to be solved with clinically relevant ligands or those that have been studied extensively in vitro. These may include bupropion, cyclophosphamide, 7-EFC, and ketamine in their native structures or as tight-binding analogs similar to the most recent CYP2B6-efavirenz analog crystal (Shah et al., 2018). As a remarkably specific (Stevens et al., 1997; Domanski et al., 1999) and recently neglected CYP2B6 substrate, RP 73401 may prove useful within X-ray crystallography or molecular docking studies for elucidating more about the putative CYP2B6 active site. A ligand-free CYP2B6 crystal structure is also still lacking. Few in silico studies have explored the enantioselectivity of CYP2B6 other than with the purported two-planar template model of its active site (Koyama and Yamazoe, 2011). Therefore, the chirality of substrates should be considered when performing X-ray crystallography or molecular docking for further insights into the stereochemical mold of the CYP2B6 active site. While crystallographic data are likely preferred over molecular docking results, the latter are still useful (Domanski et al., 1999; Bathelt et al., 2002; Niu et al., 2011; Wang et al., 2019b) and need continued performance with additional substrates for analyzing the CYP2B6 structure–function relationship, especially with lower affinity substrates that are difficult to crystallize within CYP2B6. The application of NMR-based tools (Estrada et al., 2013; Estrada et al., 2016; Bart and Scott, 2017), isothermal titration calorimetry (Zhao and Halpert, 2007), and deuterium exchange mass spectrometry (Halpert, 2011) for in silico CYP2B6 characterization will likely be advantageous for better understanding its structure–function relationship as well (Wilderman and Halpert, 2012). Above all else, more in silico work needs to be done with characterizing the functions of CYP2B6 active site residues.

As previously mentioned, Lewis and others pioneered many of the CYP2B6 structure–function studies with the use of homology models (Supplemental Table 1). Now that we have access to 13 CYP2B6 crystal structures (Table 1), however, there is a significant amount of increasingly accurate in silico findings and reasonable speculations to be made for the function of CYP2B6 active site residues in binding ligands and interacting with one another. These findings may enhance our understanding of the CYP2B6 pharmacophore for calculating QSARs, perhaps allowing an easier differentiation between CYP2B6 substrates/inhibitors and explaining why select substrates also function as inhibitors (Bumpus et al., 2005; Bumpus et al., 2006; Korhonen et al., 2007; Ekins et al., 2008; Lewis et al., 2010; Lee et al., 2018). This may also allow a more rational mutagenesis of CYP2B6 to alter its functionality in directed ways. Harnessing in tandem the power of in silico tools such as X-ray crystallography and molecular docking with in vitro techniques like site-directed mutagenesis and kinetic parameter measurement may be the key to rationalizing CYP2B6 substrate specificity, stereospecificity, and regiospecificity (Kumar et al., 2003; Kumar et al., 2007; Zhao and Halpert, 2007; Nguyen et al., 2008; Koyama and Yamazoe, 2011; Radloff et al., 2013; Watanabe et al., 2018; Wang et al., 2019b). It may be possible for polymorphic mutations surrounding the active site to translate into it and impact metabolism through modulations in protein flexibility (Zhao and Halpert, 2007; Shah et al., 2012; Wilderman and Halpert, 2012; Kobayashi et al., 2014; Shah et al., 2015; Shah et al., 2016), solubility/stability (Bumpus et al., 2005; Kumar et al., 2007; Hofmann et al., 2008; Watanabe et al., 2010; Kobayashi et al., 2014; Watanabe et al., 2018), and substrate channel access (Cojocaru et al., 2007; Shah et al., 2012; Jang et al., 2014; Lautier et al., 2016) mediated by energetically stabilizing/destabilizing and sterically favoring/hindering residue contacts (Gay et al., 2010; Watanabe et al., 2010; Halpert, 2011; Shah et al., 2011; Shah et al., 2012; Wilderman et al., 2013; Kobayashi et al., 2014; Shah et al., 2015; Shah et al., 2018; Watanabe et al., 2018). However, understanding the structure–function relationship of the CYP2B6 active site at least as well as we currently understand the structure–function relationship of CYP2B6 polymorphs may be of immense pharmaceutical, medical, environmental, and biochemical usefulness.

A multidisciplinary approach combining in silico and in vitro tools to study CYP2B6 has been successfully employed before (Domanski et al., 1999; Spatzenegger et al., 2003; Kent et al., 2006; Korhonen et al., 2007; Nguyen et al., 2008; Niu et al., 2011; Radloff et al., 2013; Gong et al., 2018; Watanabe et al., 2018; Wang et al., 2019b; Zhang et al., 2021). These studies set the precedent that strongly urges future CYP2B6 studies to use a multidisciplinary method. It may prove beneficial to systematically perform in vitro site-saturation mutagenesis of CYP2B6 active site residues and measure the corresponding catalytic data with various clinically relevant substrates or persistent organic pollutants. The changes that these mutations induce within the enzyme structure, interactions governing substrate binding/metabolism, and potentially the identity of metabolites can then be visualized and/or predicted in silico to advance and reinforce the speculations to be made about the CYP2B6 structure–function relationship. Elucidating how slight changes above the CYP2B6 heme affect substrate metabolism may even eventually allow an engineering of CYP2B6 or other P450 subfamily 2B enzymes to perform coordinated oxidative reactions that are humanly valuable (Kumar et al., 2003; Zhao and Halpert, 2007), as was accomplished with a bacterial P450 by the Arnold Laboratory (Fasan et al., 2019). More may be known about other P450 subfamily 2B enzymes like rat CYP2B1 and rabbit CYP2B4 (Zhao and Halpert, 2007) or even the CYP2B6.6 polymorph (Jinno et al., 2003; Xie et al., 2003; Crane et al., 2012; Xu et al., 2012; Li et al., 2013; Zanger and Klein, 2013; Court et al., 2014) than the CYP2B6 active site, making it evident that a similar level of knowledge about the CYP2B6 active site can be attained if the effort is dedicated toward it.

In conclusion, the fertile grounds for cultivating future CYP2B6 structure–function insights exist as a two-step plan. We advise that a multidisciplinary approach be used that takes advantage of the well-substantiated predictive power of in silico tools and the in vitro utility of site-directed/site-saturation mutagenesis paired with kinetic parameterization. Furthermore, work should focus on CYP2B6 active site residues and could even extend to those involved in POR/cyt b5 binding and electron transfer to better understand the biochemistry of CYP2B6. It is also important to consider standardizing in vitro experimental conditions for cross-study comparisons of wild-type and mutant CYP2B6 catalytic constants. The surplus of information that is still unknown about the CYP2B6 structure–function relationship could begin to be revealed by the multidisciplinary symbiosis of in silico and in vitro data to allow for more profound structural and functional speculations about CYP2B6.

Authorship Contributions

Wrote the manuscript: Angle and Cox.

References

Appiah-Opong R, de Esch I, Commandeur JN, Andarini M, and Vermeulen NP (2008) Structure-activity relationships for the inhibition of recombinant human cytochromes P450 by curcumin analogues. *Eur J Med Chem* **43:**1621–1631.

Ariyoshi N, Ohara M, Kaneko M, Afuso S, Kumamoto T, Nakamura H, Ishii I, Ishikawa T, and Kitada M (2011) Q172H replacement overcomes effects on the metabolism of cyclophosphamide and efavirenz caused by CYP2B6 variant with Arg262. *Drug Metab Dispos* **39:**2045–2048.

Avery LB, VanAusdall JL, Hendrix CW, and Bumpus NN (2013) Compartmentalization and antiviral effect of efavirenz metabolites in blood plasma, seminal plasma, and cerebrospinal fluid. *Drug Metab Dispos* **41:**422–429.

Bamfo NO, Lu JBL, and Desta Z (2022) Stereoselective metabolism of bupropion to active metabolites in cellular fractions of human liver and intestine. *Drug Metab Dispos* DMD-AR-2022-000867.

Bart AG and Scott EE (2017) Structural and functional effects of cytochrome b_5 interactions with human cytochrome P450 enzymes. *J Biol Chem* **292:**20818–20833.

Bathelt C, Schmid RD, and Pleiss J (2002) Regioselectivity of CYP2B6: homology modeling, molecular dynamics simulation, docking. *J Mol Model* **8:**327–335.

Bloom AJ, Wang PF, and Kharasch ED (2019) Nicotine oxidation by genetic variants of CYP2B6 and in human brain microsomes. *Pharmacol Res Perspect* **7:**e00468.

Bolla L, Srivastava P, Ravichandiran V, and Nanjappan SK (2021) Cytochrome P450 and P-gp mediated herb-drug interactions and molecular docking studies of garcinol. *Membranes (Basel)* **11:**992.

Bumpus NN and Hollenberg PF (2008) Investigation of the mechanisms underlying the differential effects of the K262R mutation of P450 2B6 on catalytic activity. *Mol Pharmacol* **74:** 990–999.

Bumpus NN, Kent UM, and Hollenberg PF (2006) Metabolism of efavirenz and 8-hydroxyefavirenz by P450 2B6 leads to inactivation by two distinct mechanisms. *J Pharmacol Exp Ther* **318:** 345–351.

Bumpus NN, Sridar C, Kent UM, and Hollenberg PF (2005) The naturally occurring cytochrome P450 (P450) 2B6 K262R mutant of P450 2B6 exhibits alterations in substrate metabolism and inactivation. *Drug Metab Dispos* **33:**795–802.

Calinski DM, Zhang H, Ludeman S, Dolan ME, and Hollenberg PF (2015) Hydroxylation and N-dechloroethylation of ifosfamide and deuterated ifosfamide by the human cytochrome p450s and their commonly occurring polymorphisms. *Drug Metab Dispos* **43:**1084–1090.

Chen C, Liu J, Halpert JR, and Wilderman PR (2018) Use of phenoxyaniline analogues to generate biochemical insights into the interaction of polybrominated diphenyl ether with CYP2B enzymes. *Biochemistry* **57:**817–826.

Cojocaru V, Winn PJ, and Wade RC (2007) The ins and outs of cytochrome P450s. *Biochim Biophys Acta* **1770:**390–401.

Coles R and Kharasch ED (2008) Stereoselective metabolism of bupropion by cytochrome P4502B6 (CYP2B6) and human liver microsomes. *Pharm Res* **25:**1405–1411.

Court MH, Almutairi FE, Greenblatt DJ, Hazarika S, Sheng H, Klein K, Zanger UM, Bourgea J, Patten CJ, and Kwara A (2014) Isoniazid mediates the CYP2B6*6 genotype-dependent interaction between efavirenz and antituberculosis drug therapy through mechanism-based inactivation of CYP2A6. *Antimicrob Agents Chemother* **58:**4145–4152.

Cox PM and Bumpus NN (2014) Structure-activity studies reveal the oxazinone ring is a determinant of cytochrome P450 2B6 activity toward efavirenz. *ACS Med Chem Lett* **5:**1156–1161.

Cox PM and Bumpus NN (2016) Single heteroatom substitutions in the efavirenz oxazinone ring impact metabolism by CYP2B6. *ChemMedChem* **11:**2630–2637.

Crane AL, Klein K, Zanger UM, and Olson JR (2012) Effect of CYP2B6*6 and CYP2C19*2 genotype on chlorpyrifos metabolism. *Toxicology* **293:**115–122.

Crettol S, Déglon JJ, Besson J, Croquette-Krokkar M, Gothuey I, Hämmig R, Monnat M, Hüttemann H, Baumann P, and Eap CB (2005) Methadone enantiomer plasma levels, CYP2B6, CYP2C19, and CYP2C9 genotypes, and response to treatment. *Clin Pharmacol Ther* **78:**593–604.

de Graaf C, Vermeulen NP, and Feenstra KA (2005) Cytochrome p450 in silico: an integrative modeling approach. *J Med Chem* **48:**2725–2755.

Desta Z, El-Boraie A, Gong L, Somogyi AA, Lauschke VM, Dandara C, Klein K, Miller NA, Klein TE, Tyndale RF et al. (2021) PharmVar GeneFocus: CYP2B6. *Clin Pharmacol Ther* **110:**82–97.

Desta Z, Moaddel R, Ogburn ET, Xu C, Ramamoorthy A, Venkata SL, Sanghvi M, Goldberg ME, Torjman MC, and Wainer IW (2012) Stereoselective and regiospecific hydroxylation of ketamine and norketamine. *Xenobiotica* **42:**1076–1087.

Desta Z, Saussele T, Ward B, Blievernicht J, Li L, Klein K, Flockhart DA, and Zanger UM (2007) Impact of CYP2B6 polymorphism on hepatic efavirenz metabolism in vitro. *Pharmacogenomics* **8:**547–558.

Dmitriev AV, Rudik AV, Karasev DA, Pogodin PV, Lagunin AA, Filimonov DA, and Poroikov VV (2021) In silico prediction of drug-drug interactions mediated by cytochrome P450 isoforms. *Pharmaceutics* **13:**538.

Domanski TL and Halpert JR (2001) Analysis of mammalian cytochrome P450 structure and function by site-directed mutagenesis. *Curr Drug Metab* **2:**117–137.

Domanski TL, Schultz KM, Roussel F, Stevens JC, and Halpert JR (1999) Structure-function analysis of human cytochrome P-450 2B6 using a novel substrate, site-directed mutagenesis, and molecular modeling. *J Pharmacol Exp Ther* **290:**1141–1147.

Ekins S, Bravi G, Ring BJ, Gillespie TA, Gillespie JS, Vandenbranden M, Wrighton SA, and Wikel JH (1999) Three-dimensional quantitative structure activity relationship analyses of substrates for CYP2B6. *J Pharmacol Exp Ther* **288:**21–29.

Ekins S, Iyer M, Krasowski MD, and Kharasch ED (2008) Molecular characterization of CYP2B6 substrates. *Curr Drug Metab* **9:**363–373.

Ekins S and Wrighton SA (1999) The role of CYP2B6 in human xenobiotic metabolism. *Drug Metab Rev* **31:**719–754.

El-Serafi I, Afsharian P, Moshfegh A, Hassan M, and Terelius Y (2015) Cytochrome P450 oxidoreductase influences CYP2B6 activity in cyclophosphamide bioactivation. *PLoS One* **10:**e0141979.

Erratico CA, Deo AK, and Bandiera SM (2015) Regioselective versatility of monooxygenase reactions catalyzed by CYP2B6 and CYP3A4: examples with single substrates. *Adv Exp Med Biol* **851:**131–149.

Estrada DF, Laurence JS, and Scott EE (2013) Substrate-modulated cytochrome P450 17A1 and cytochrome b5 interactions revealed by NMR. *J Biol Chem* **288:**17008–17018.

Estrada DF, Laurence JS, and Scott EE (2016) Cytochrome P450 17A1 interactions with the FMN domain of its reductase as characterized by NMR. *J Biol Chem* **291:**3990–4003.

Fasan R, Jennifer Kan SB, and Zhao H (2019) A continuing career in biocatalysis: Frances H. Arnold. *ACS Catal* **9:**9775–9788.

Gadel S, Crafford A, Regina K, and Kharasch ED (2013) Methadone N-demethylation by the common CYP2B6 allelic variant CYP2B6.6. *Drug Metab Dispos* **41:**709–713.

Gadel S, Friedel C, and Kharasch ED (2015) Differences in methadone metabolism by CYP2B6 variants. *Drug Metab Dispos* **43:**994–1001.

Gay SC, Shah MB, Talakad JC, Maekawa K, Roberts AG, Wilderman PR, Sun L, Yang JY, Huelga SC, Hong WX et al. (2010) Crystal structure of a cytochrome P450 2B6 genetic variant in complex with the inhibitor 4-(4-chlorophenyl)imidazole at 2.0-A resolution. *Mol Pharmacol* **77:**529–538.

Gerber JG, Rhodes RJ, and Gal J (2004) Stereoselective metabolism of methadone N-demethylation by cytochrome P4502B6 and 2C19. *Chirality* **16:**36–44.

Gong EC, Chea S, Balupuri A, Kang NS, Chin YW, and Choi YH (2018) Enzyme kinetics and molecular docking studies on cytochrome 2B6, 2C19, 2E1, and 3A4 activities by sauchinone. *Molecules* **23:**555.

Gotoh O (1992) Substrate recognition sites in cytochrome P450 family 2 (CYP2) proteins inferred from comparative analyses of amino acid and coding nucleotide sequences. *J Biol Chem* **267:**83–90.

Gross MS, Butryn DM, McGarrigle BP, Aga DS, and Olson JR (2015) Primary role of cytochrome P450 2B6 in the oxidative metabolism of 2,2′,4,4′,6-pentabromodiphenyl ether (BDE-100) to hydroxylated BDEs. *Chem Res Toxicol* **28:**672–681.

Guengerich FP (2017) Intersection of the roles of cytochrome P450 enzymes with xenobiotic and endogenous substrates: relevance to toxicity and drug interactions. *Chem Res Toxicol* **30:**2–12.

Halpert JR (2011) Structure and function of cytochromes P450 2B: from mechanism-based inactivators to X-ray crystal structures and back. *Drug Metab Dispos* **39:**1113–1121.

Hirakawa S, Miyawaki T, Hori T, Kajiwara J, Katsuki S, Hirano M, Yoshinouchi Y, Iwata H, Mitoma C, and Furue M (2018) Accumulation properties of polychlorinated biphenyl congeners in Yusho patients and prediction of their cytochrome P450-dependent metabolism by in silico analysis. *Environ Sci Pollut Res Int* **25:**16455–16463.

Hodgson E and Rose RL (2007) The importance of cytochrome P450 2B6 in the human metabolism of environmental chemicals. *Pharmacol Ther* **113:**420–428.

Hofmann MH, Blievernicht JK, Klein K, Saussele T, Schaeffeler E, Schwab M, and Zanger UM (2008) Aberrant splicing caused by single nucleotide polymorphism c.516G>T [Q172H], a marker of CYP2B6*6, is responsible for decreased expression and activity of CYP2B6 in liver. *J Pharmacol Exp Ther* **325:**284–292.

Honda M, Muroi Y, Tamaki Y, Saigusa D, Suzuki N, Tomioka Y, Matsubara Y, Oda A, Hirasawa N, and Hiratsuka M (2011) Functional characterization of CYP2B6 allelic variants in demethylation of antimalarial artemether. *Drug Metab Dispos* **39:**1860–1865.

Imaishi H and Goto T (2018) Effect of genetic polymorphism of human CYP2B6 on the metabolic activation of chlorpyrifos. *Pestic Biochem Physiol* **144:**42–48.

Jang HH, Davydov DR, Lee GY, Yun CH, and Halpert JR (2014) The role of cytochrome P450 2B6 and 2B4 substrate access channel residues predicted based on crystal structures of the amlodipine complexes. *Arch Biochem Biophys* **545:**100–107.

Jinno H, Tanaka-Kagawa T, Ohno A, Makino Y, Matsushima E, Hanioka N, and Ando M (2003) Functional characterization of cytochrome P450 2B6 allelic variants. *Drug Metab Dispos* **31:**398–403.

Kent UM, Lin HL, Noon KR, Harris DL, and Hollenberg PF (2006) Metabolism of bergamottin by cytochromes P450 2B6 and 3A5. *J Pharmacol Exp Ther* **318:**992–1005.

Klein K, Lang T, Saussele T, Barbosa-Sicard E, Schunck WH, Eichelbaum M, Schwab M, and Zanger UM (2005) Genetic variability of CYP2B6 in populations of African and Asian origin: allele frequencies, novel functional variants, and possible implications for anti-HIV therapy with efavirenz. *Pharmacogenet Genomics* **15:**861–873.

Kobayashi K, Abe S, Nakajima M, Shimada N, Tani M, Chiba K, and Yamamoto T (1999) Role of human CYP2B6 in S-mephobarbital N-demethylation. *Drug Metab Dispos* **27:**1429–1433.

Kobayashi K, Takahashi O, Hiratsuka M, Yamaotsu N, Hirono S, Watanabe Y, and Oda A (2014) Evaluation of influence of single nucleotide polymorphisms in cytochrome P450 2B6 on substrate recognition using computational docking and molecular dynamics simulation. *PLoS One* **9:**e96789.

Korhonen LE, Turpeinen M, Rahnasto M, Wittekindt C, Poso A, Pelkonen O, Raunio H, and Juvonen RO (2007) New potent and selective cytochrome P450 2B6 (CYP2B6) inhibitors based on three-dimensional quantitative structure-activity relationship (3D-QSAR) analysis. *Br J Pharmacol* **150:**932–942.

Koyama N and Yamazoe Y (2011) Development of two-dimensional template system for the prediction of CYP2B6-mediated reaction sites. *Drug Metab Pharmacokinet* **26:**309–330.

Kumar S, Scott EE, Liu H, and Halpert JR (2003) A rational approach to re-engineer cytochrome P450 2B1 regioselectivity based on the crystal structure of cytochrome P450 2C5. *J Biol Chem* **278:**17178–17184.

Kumar S, Zhao Y, Sun L, Negi SS, Halpert JR, and Muralidhara BK (2007) Rational engineering of human cytochrome P450 2B6 for enhanced expression and stability: importance of a Leu264->Phe substitution. *Mol Pharmacol* **72:**1191–1199.

Lang T, Klein K, Richter T, Zibat A, Kerb R, Eichelbaum M, Schwab M, and Zanger UM (2004) Multiple novel nonsynonymous CYP2B6 gene polymorphisms in Caucasians: demonstration of phenotypic null alleles. *J Pharmacol Exp Ther* **311:**34–43.

Langmia IM, Just KS, Yamoune S, Brockmöller J, Masimirembwa C, and Stingl JC (2021) CYP2B6 functional variability in drug metabolism and exposure across populations-implication for drug safety, dosing, and individualized therapy. *Front Genet* **12:**692234.

Lautier T, Urban P, Loeper J, Jezequel L, Pompon D, and Truan G (2016) Ordered chimerogenesis applied to CYP2B P450 enzymes. *Biochim Biophys Acta* **1860:**1395–1403.

Lee Y, Park HG, Kim V, Cho MA, Kim H, Ho TH, Cho KS, Lee IS, and Kim D (2018) Inhibitory effect of α-terpinyl acetate on cytochrome P450 2B6 enzymatic activity. *Chem Biol Interact* **289:**90–97.

Lewis DF (1999) Homology modelling of human cytochromes P450 involved in xenobiotic metabolism and rationalization of substrate selectivity. *Exp Toxicol Pathol* **51:**369–374.

Lewis DF (2000) On the recognition of mammalian microsomal cytochrome P450 substrates and their characteristics: towards the prediction of human p450 substrate specificity and metabolism. *Biochem Pharmacol* **60:**293–306.

Lewis DF (2003) Essential requirements for substrate binding affinity and selectivity toward human CYP2 family enzymes. *Arch Biochem Biophys* **409:**32–44.

Lewis DF, Ito Y, and Goldfarb PS (2006) Investigating human P450s involved in drug metabolism via homology with high-resolution P450 crystal structures of the CYP2C subfamily. *Curr Drug Metab* **7:**589–598.
Lewis DF, Ito Y, and Lake BG (2010) Quantitative structure-activity relationships (QSARs) for inhibitors and substrates of CYP2B enzymes: importance of compound lipophilicity in explanation of potency differences. *J Enzyme Inhib Med Chem* **25:**679–684.
Lewis DF and Lake BG (1997) Molecular modelling of mammalian CYP2B isoforms and their interaction with substrates, inhibitors and redox partners. *Xenobiotica* **27:**443–478.
Lewis DF, Lake BG, and Dickins M (2004) Quantitative structure-activity relationships within a homologous series of 7-alkoxyresorufins exhibiting activity towards CYP1A and CYP2B enzymes: molecular modelling studies on key members of the resorufin series with CYP2C5-derived models of human CYP1A1, CYP1A2, CYP2B6 and CYP3A4. *Xenobiotica* **34:**501–513.
Lewis DF, Lake BG, Dickins M, Eddershaw PJ, Tarbit MH, and Goldfarb PS (1999) Molecular modelling of CYP2B6, the human CYP2B isoform, by homology with the substrate-bound CYP102 crystal structure: evaluation of CYP2B6 substrate characteristics, the cytochrome b5 binding site and comparisons with CYP2B1 and CYP2B4. *Xenobiotica* **29:**361–393.
Lewis DF, Lake BG, Dickins M, and Goldfarb PS (2002) Molecular modelling of CYP2B6 based on homology with the CYP2C5 crystal structure: analysis of enzyme-substrate interactions. *Drug Metabol Drug Interact* **19:**115–135.
Lewis DF, Modi S, and Dickins M (2001) Quantitative structure-activity relationships (QSARs) within substrates of human cytochromes P450 involved in drug metabolism. *Drug Metabol Drug Interact* **18:**221–242.
Li J, Zhou Y, Tang Y, Li W, and Tu Y (2020) Dissecting the structural plasticity and dynamics of cytochrome P450 2B4 by molecular dynamics simulations. *J Chem Inf Model* **60:**5026–5035.
Li Y, Coller JK, Hutchinson MR, Klein K, Zanger UM, Stanley NJ, Abell AD, and Somogyi AA (2013) The CYP2B6*6 allele significantly alters the N-demethylation of ketamine enantiomers in vitro. *Drug Metab Dispos* **41:**1264–1272.
Lin HL, Zhang H, Kenaan C, and Hollenberg PF (2016) Roles of residues F206 and V367 in human CYP2B6: effects of mutations on androgen hydroxylation, mechanism-based inactivation, and reversible inhibition. *Drug Metab Dispos* **44:**1771–1779.
Lin HL, Zhang H, Pratt-Hyatt MJ, and Hollenberg PF (2011) Thr302 is the site for the covalent modification of human cytochrome P450 2B6 leading to mechanism-based inactivation by tert-butylphenylacetylene. *Drug Metab Dispos* **39:**2431–2439.
Liu J, Shah MB, Zhang Q, Stout CD, Halpert JR, and Wilderman PR (2016) Coumarin derivatives as substrate probes of mammalian cytochromes P450 2B4 and 2B6: assessing the importance of 7-alkoxy chain length, halogen substitution, and non-active site mutations. *Biochemistry* **55:**1997–2007.
Lu H, Wang JJ, Chan KK, and Philip PA (2006) Stereoselectivity in metabolism of ifosfamide by CYP3A4 and CYP2B6. *Xenobiotica* **36:**367–385.
Maldonado-Rojas W, Rivera-Julio K, Olivero-Verbel J, and Aga DS (2016) Mechanisms of interaction between persistent organic pollutants (POPs) and CYP2B6: an in silico approach. *Chemosphere* **159:**113–125.
Miles JS, Spurr NK, Gough AC, Jowett T, McLaren AW, Brook JD, and Wolf CR (1988) A novel human cytochrome P450 gene (P450IIB): chromosomal localization and evidence for alternative splicing. *Nucleic Acids Res* **16:**5783–5795.
Mise S, Haga Y, Itoh T, Kato A, Fukuda I, Goto E, Yamamoto K, Yabu M, Matsumura C, Nakano T et al. (2016) From the cover: structural determinants of the position of 2,3′,4,4′,5-pentachlorobiphenyl (CB118) hydroxylation by mammalian cytochrome P450 monooxygenases. *Toxicol Sci* **152:**340–348.
Mo SL, Liu YH, Duan W, Wei MQ, Kanwar JR, and Zhou SF (2009) Substrate specificity, regulation, and polymorphism of human cytochrome P450 2B6. *Curr Drug Metab* **10:**730–753.
Naidoo P, Chetty VV, and Chetty M (2014) Impact of CYP polymorphisms, ethnicity and sex differences in metabolism on dosing strategies: the case of efavirenz. *Eur J Clin Pharmacol* **70:**379–389.
Nebert DW, Wikvall K, and Miller WL (2013) Human cytochromes P450 in health and disease. *Philos Trans R Soc Lond B Biol Sci* **368:**20120431.
Nelson DR (2011) Progress in tracing the evolutionary paths of cytochrome P450. *Biochim Biophys Acta* **1814:**14–18.
Nguyen TA, Tychopoulos M, Bichat F, Zimmermann C, Flinois JP, Diry M, Ahlberg E, Delaforge M, Corcos L, Beaune P et al. (2008) Improvement of cyclophosphamide activation by CYP2B6 mutants: from in silico to ex vivo. *Mol Pharmacol* **73:**1122–1133.
Niu RJ, Zheng QC, Zhang JL, and Zhang HX (2011) Analysis of clinically relevant substrates of CYP2B6 enzyme by computational methods. *J Mol Model* **17:**2839–2846.
Niwa T, Murayama N, and Yamazaki H (2011) Stereoselectivity of human cytochrome p450 in metabolic and inhibitory activities. *Curr Drug Metab* **12:**549–569.
Ogburn ET, Jones DR, Masters AR, Xu C, Guo Y, and Desta Z (2010) Efavirenz primary and secondary metabolism in vitro and in vivo: identification of novel metabolic pathways and cytochrome P450 2A6 as the principal catalyst of efavirenz 7-hydroxylation. *Drug Metab Dispos* **38:**1218–1229.
Qian J, Li Y, Zhang X, Chen D, Han M, Xu T, Chen B, Hu G, and Li J (2022) Herbacetin broadly blocks the activities of CYP450s by different inhibitory mechanisms. *Planta Med* **88:**507–517
Raccor BS, Claessens AJ, Dinh JC, Park JR, Hawkins DS, Thomas SS, Makar KW, McCune JS, and Totah RA (2012) Potential contribution of cytochrome P450 2B6 to hepatic 4-hydroxycyclophosphamide formation in vitro and in vivo. *Drug Metab Dispos* **40:**54–63.
Radloff R, Gras A, Zanger UM, Masquelier C, Arumugam K, Karasi JC, Arendt V, Seguin-Devaux C, and Klein K (2013) Novel CYP2B6 enzyme variants in a Rwandese population: functional characterization and assessment of in silico prediction tools. *Hum Mutat* **34:**725–734.
Roy P, Tretyakov O, Wright J, and Waxman DJ (1999) Stereoselective metabolism of ifosfamide by human P-450s 3A4 and 2B6. Favorable metabolic properties of R-enantiomer. *Drug Metab Dispos* **27:**1309–1318.
Sager JE, Price LS, and Isoherranen N (2016) Stereoselective metabolism of bupropion to OH-bupropion, threohydrobupropion, erythrohydrobupropion, and 4′-OH-bupropion in vitro. *Drug Metab Dispos* **44:**1709–1719.
Salonen JS, Nyman L, Boobis AR, Edwards RJ, Watts P, Lake BG, Price RJ, Renwick AB, Gómez-Lechón MJ, Castell JV et al. (2003) Comparative studies on the cytochrome p450-associated metabolism and interaction potential of selegiline between human liver-derived in vitro systems. *Drug Metab Dispos* **31:**1093–1102.
Scott EE, Spatzenegger M, and Halpert JR (2001) A truncation of 2B subfamily cytochromes P450 yields increased expression levels, increased solubility, and decreased aggregation while retaining function. *Arch Biochem Biophys* **395:**57–68.
Shah MB, Liu J, Huo L, Zhang Q, Dearing MD, Wilderman PR, Szklarz GD, Stout CD, and Halpert JR (2016) Structure-function analysis of mammalian CYP2B enzymes using 7-substituted coumarin derivatives as probes: utility of crystal structures and molecular modeling in understanding xenobiotic metabolism. *Mol Pharmacol* **89:**435–445.
Shah MB, Liu J, Zhang Q, Stout CD, and Halpert JR (2017) Halogen-π interactions in the cytochrome P450 active site: structural insights into human CYP2B6 substrate selectivity. *ACS Chem Biol* **12:**1204–1210.
Shah MB, Pascual J, Zhang Q, Stout CD, and Halpert JR (2011) Structures of cytochrome P450 2B6 bound to 4-benzylpyridine and 4-(4-nitrobenzyl)pyridine: insight into inhibitor binding and rearrangement of active site side chains. *Mol Pharmacol* **80:**1047–1055.
Shah MB, Wilderman PR, Liu J, Jang HH, Zhang Q, Stout CD, and Halpert JR (2015) Structural and biophysical characterization of human cytochromes P450 2B6 and 2A6 bound to volatile hydrocarbons: analysis and comparison. *Mol Pharmacol* **87:**649–659.
Shah MB, Wilderman PR, Pascual J, Zhang Q, Stout CD, and Halpert JR (2012) Conformational adaptation of human cytochrome P450 2B6 and rabbit cytochrome P450 2B4 revealed upon binding multiple amlodipine molecules. *Biochemistry* **51:**7225–7238.
Shah MB, Zhang Q, and Halpert JR (2018) Crystal structure of CYP2B6 in complex with an efavirenz analog. *Int J Mol Sci* **19:**1025.
Spatzenegger M, Liu H, Wang Q, Debarber A, Koop DR, and Halpert JR (2003) Analysis of differential substrate selectivities of CYP2B6 and CYP2E1 by site-directed mutagenesis and molecular modeling. *J Pharmacol Exp Ther* **304:**477–487.
Stevens JC, White RB, Hsu SH, and Martinet M (1997) Human liver CYP2B6-catalyzed hydroxylation of RP 73401. *J Pharmacol Exp Ther* **282:**1389–1395.
Talakad JC, Shah MB, Walker GS, Xiang C, Halpert JR, and Dalvie D (2011) Comparison of in vitro metabolism of ticlopidine by human cytochrome P450 2B6 and rabbit cytochrome P450 2B4. *Drug Metab Dispos* **39:**539–550.
Totah RA, Allen KE, Sheffels P, Whittington D, and Kharasch ED (2007) Enantiomeric metabolic interactions and stereoselective human methadone metabolism. *J Pharmacol Exp Ther* **321:**389–399.
Totah RA, Sheffels P, Roberts T, Whittington D, Thummel K, and Kharasch ED (2008) Role of CYP2B6 in stereoselective human methadone metabolism. *Anesthesiology* **108:**363–374.
Turpeinen M and Zanger UM (2012) Cytochrome P450 2B6: function, genetics, and clinical relevance. *Drug Metabol Drug Interact* **27:**185–197.
Wang G, Li Y, Sun W, Wang Z, Chen D, Shu S, Jin J, Mahoo J, Pan L, Hu G et al. (2020a) Cytochrome P450-mediated metabolic characterization of a mono-carbonyl curcumin analog WZ35. *Pharmacology* **105:**79–89.
Wang H and Tompkins LM (2008) CYP2B6: new insights into a historically overlooked cytochrome P450 isozyme. *Curr Drug Metab* **9:**598–610.
Wang J, Sönnerborg A, Rane A, Josephson F, Lundgren S, Ståhle L, and Ingelman-Sundberg M (2006) Identification of a novel specific CYP2B6 allele in Africans causing impaired metabolism of the HIV drug efavirenz. *Pharmacogenet Genomics* **16:**191–198.
Wang PF, Neiner A, and Kharasch ED (2018) Stereoselective ketamine metabolism by genetic variants of cytochrome P450 CYP2B6 and cytochrome P450 oxidoreductase. *Anesthesiology* **129:**756–768.
Wang PF, Neiner A, and Kharasch ED (2019a) Efavirenz metabolism: influence of polymorphic CYP2B6 variants and stereochemistry. *Drug Metab Dispos* **47:**1195–1205.
Wang PF, Neiner A, and Kharasch ED (2020b) Stereoselective bupropion hydroxylation by cytochrome P450 CYP2B6 and cytochrome P450 oxidoreductase genetic variants. *Drug Metab Dispos* **48:**438–445.
Wang PF, Neiner A, Lane TR, Zorn KM, Ekins S, and Kharasch ED (2019b) Halogen substitution influences ketamine metabolism by cytochrome P450 2B6: in vitro and computational approaches. *Mol Pharm* **16:**898–906.
Wang Q and Halpert JR (2002) Combined three-dimensional quantitative structure-activity relationship analysis of cytochrome P450 2B6 substrates and protein homology modeling. *Drug Metab Dispos* **30:**86–95.
Ward BA, Gorski JC, Jones DR, Hall SD, Flockhart DA, and Desta Z (2003) The cytochrome P450 2B6 (CYP2B6) is the main catalyst of efavirenz primary and secondary metabolism: implication for HIV/AIDS therapy and utility of efavirenz as a substrate marker of CYP2B6 catalytic activity. *J Pharmacol Exp Ther* **306:**287–300.
Watanabe T, Saito T, Rico EMG, Hishinuma E, Kumondai M, Maekawa M, Oda A, Saigusa D, Saito S, Yasuda J et al. (2018) Functional characterization of 40 CYP2B6 allelic variants by assessing efavirenz 8-hydroxylation. *Biochem Pharmacol* **156:**420–430.
Watanabe T, Sakuyama K, Sasaki T, Ishii Y, Ishikawa M, Hirasawa N, and Hiratsuka M (2010) Functional characterization of 26 CYP2B6 allelic variants (CYP2B6.2-CYP2B6.28, except CYP2B6.22). *Pharmacogenet Genomics* **20:**459–462.
Wilderman PR and Halpert JR (2012) Plasticity of CYP2B enzymes: structural and solution biophysical methods. *Curr Drug Metab* **13:**167–176.
Wilderman PR, Shah MB, Jang HH, Stout CD, and Halpert JR (2013) Structural and thermodynamic basis of (+)-α-pinene binding to human cytochrome P450 2B6. *J Am Chem Soc* **135:**10433–10440.
Xie HJ, Yasar U, Lundgren S, Griskevicius L, Terelius Y, Hassan M, and Rane A (2003) Role of polymorphic human CYP2B6 in cyclophosphamide bioactivation. *Pharmacogenomics J* **3:**53–61.
Xu C, Ogburn ET, Guo Y, and Desta Z (2012) Effects of the CYP2B6*6 allele on catalytic properties and inhibition of CYP2B6 in vitro: implication for the mechanism of reduced efavirenz metabolism and other CYP2B6 substrates in vivo. *Drug Metab Dispos* **40:**717–725.
Yoo SE, Yi M, Kim WY, Cho SA, Lee SS, Lee SJ, and Shin JG (2019) Influences of cytochrome b5 expression and its genetic variant on the activity of CYP2C9, CYP2C19 and CYP3A4. *Drug Metab Pharmacokinet* **34:**201–208.
Zanger UM and Klein K (2013) Pharmacogenetics of cytochrome P450 2B6 (CYP2B6): advances on polymorphisms, mechanisms, and clinical relevance. *Front Genet* **4:**24.
Zanger UM, Klein K, Saussele T, Blievernicht J, Hofmann MH, and Schwab M (2007) Polymorphic CYP2B6: molecular mechanisms and emerging clinical significance. *Pharmacogenomics* **8:**743–759.
Zhang H, Sanidad KZ, Zhu L, Parsonnet J, Haggerty TD, Zhang G, and Cai Z (2021) Frequent occurrence of triclosan hydroxylation in mammals: a combined theoretical and experimental investigation. *J Hazard Mater* **407:**124803.

Zhang H, Sridar C, Kenaan C, Amunugama H, Ballou DP, and Hollenberg PF (2011) Polymorphic variants of cytochrome P450 2B6 (CYP2B6.4-CYP2B6.9) exhibit altered rates of metabolism for bupropion and efavirenz: a charge-reversal mutation in the K139E variant (CYP2B6.8) impairs formation of a functional cytochrome p450-reductase complex. *J Pharmacol Exp Ther* **338:**803–809.
Zhao Y and Halpert JR (2007) Structure-function analysis of cytochromes P450 2B. *Biochim Biophys Acta* **1770:**402–412.

Address correspondence to: Philip M. Cox, Department of Biology and Chemistry, Azusa Pacific University College of Liberal Arts and Sciences, 675 E. Foothill Blvd., Segerstrom Science Center Room 301, Azusa, CA 91702. E-mail: pcox@apu.edu

Multidisciplinary Insights into the Structure-Function Relationship of the CYP2B6 Active Site

(Supplemental Tables)

Drug Metabolism and Disposition

Manuscript #: DMD-MR-2022-000853

Ethan D. Angle[1,2] and Philip M. Cox[1]

[1] Department of Biology and Chemistry (E.D.A., P.M.C.)

College of Liberal Arts and Sciences, Azusa Pacific University, Azusa, CA, USA

[2] Roy J. and Lucille A. Carver College of Medicine (E.D.A.)

University of Iowa, Iowa City, IA, USA

Supplemental Table 1. Historical *in silico* insights of predicted active site amino acids and their topological locations around various ligands within P450 homology modeled CYP2B6.

Homology Model of CYP2B6	PDB ID	Ligand Bound/Docked	Predicted Active Site Amino Acids[a,b]	Topological Location in CYP2B6	Reference
CYP102	Not Reported	Tamoxifen	**F206,** **S210,** **F297,** Q473	Helix F, F-F' loop, Helix I, C-terminal coil	(Lewis and Lake, 1997)
	1FAG	4-trifluoromethyl-7-ethoxycoumarin	T205, **F206,** **S294,** **T302,** **L363,** Q473, **C475**	Helix F, Helix F, Helix I, Helix I, K-K' loop, C-terminal coil, β4-1 strand	(Lewis et al., 1999)
	1FAG	*(S)*-mephenytoin	R109, **I114,** **F206,** **T302,** Q473, E474, **C475**	B'-C loop, B'-C loop, Helix F, Helix I, C-terminal coil, β4-1 strand, β4-1 strand	(Lewis et al., 1999)
	1FAG	Bupropion	**I114**, T205, **F206,** **L363,** Q473, E474	B'-C loop, Helix F, Helix F, K-K' loop, C-terminal coil, β4-1 strand	(Lewis et al., 1999)
	1FAG	Testosterone	**I101,** **I114,** T205, **F206,** **I209,** **T302,** **L363,** E474, **C475**	B-B' loop, B'-C loop, Helix F, Helix F, Helix F, Helix I, K-K' loop, β4-1 strand, β4-1 strand	(Lewis et al., 1999)
	1FAG	Antipyrine	**I114,** **F206,** **T302,** **C475**	B'-C loop, Helix F, Helix I, β4-1 strand	(Lewis et al., 1999)
	1FAG	Diazepam	**I114,** **F206,** **T302,** **L363,** Q473, E474, **C475**	B'-C loop, Helix F, Helix I, K-K' loop, C-terminal coil, β4-1 strand, β4-1 strand	(Lewis et al., 1999)
	1FAG	Methoxychlor	**I114,** T205, **F206,** **T302,** Q473,	B'-C loop, Helix F, Helix F, Helix I, C-terminal coil,	(Lewis et al., 1999)

			C475	β4-1 strand	
	1FAG	Cyclophosphamide	**I114,** **S294,** **T302,** **L363,** Q473, **C475**	B'-C loop, Helix I, Helix I, K-K' loop, C-terminal coil, β4-1 strand	(Lewis et al., 1999)
	1FAG	Ifosfamide	**S294,** **A298,** **T302,** **L363,** E474 **C475**	Helix I, Helix I, Helix I, K-K' loop, β4-1 strand, β4-1 strand	(Lewis et al., 1999)
	1FAG	7-pentoxyresorufin	**I114,** T205, **F206,** **T302,** **L363,** M365, **C475**	B'-C loop, Helix F, Helix F, Helix I, K-K' loop, K-K' loop, β4-1 strand	(Lewis et al., 1999)
	1FAG	7-benzyloxyresorufin	**I101,** **I114,** T205, **F206,** **T302,** **L363,** M365, **C475**	B-B' loop, B'-C loop, Helix F, Helix F, Helix I, K-K' loop, K-K' loop, β4-1 strand	(Lewis et al., 1999)
	1FAG	Orphenadrine	**I114,** **F115,** **F297,** **T302,** **L363,** E474	B'-C loop, B'-C loop, Helix I, K-K' loop, Helix I, β4-1 strand	(Lewis et al., 1999)
	1FAG	Selegiline	**I114,** **F115,** **F206,** **A298,** **T302,** **L363**	B'-C loop, B'-C loop, Helix F, Helix I, K-K' loop, Helix I	(Salonen et al., 2003)
CYP2C5	1DT6	4-trifluoromethyl-7-ethoxycoumarin	**I114,** **F115,** T205, **F206,** **S294,** **F297,** **T302,** **L363,** **V477**	B'-C loop, B'-C loop, Helix F, Helix F, Helix I, Helix I, Helix I, K-K' loop, C-terminal coil	(Lewis et al., 2002)
	1DT6	4-trifluoromethyl-7-ethoxycoumarin (orientation 1)	**F206,** **A298,** **E301,** **T302,** T305, T306,	Helix F, Helix I, Helix I, Helix I, Helix I, Helix I,	(Wang and Halpert, 2002)

			L362, **L363,** **V367,** **V477,** **G478,** **K479**	K-K' loop, K-K' loop, K-K' loop, C-terminal coil, C-terminal coil, β4-2 strand	
	1DT6	4-trifluoromethyl-7-ethoxycoumarin (orientation 2)	**K100,** M103, **I114,** **F115,** **F206,** **F297,** **A298,** **T302,** **V367,** **V477**	B-B' loop, B-B' loop, B'-C loop, B'-C loop, Helix F, Helix I, Helix I, Helix I, K-K' loop, C-terminal coil	(Wang and Halpert, 2002)
	1DT6	7-benzyloxyresorufin	**I114,** **F115,** **F206,** **F297,** **A298,** **E301,** **T302,** **L363,** **V367,** **V477,** **G478**	B'-C loop, B'-C loop, Helix F, Helix I, Helix I, Helix I, Helix I, K-K' loop, K-K' loop, C-terminal coil, C-terminal coil	(Wang and Halpert, 2002)
	1DT6	Cyclophosphamide	**I114,** **F115,** **F206,** **I209,** L216, **S294,** **F297,** **A298,** **T302,** **L363,** **V367,** **V477**	B'-C loop, B'-C loop, Helix F, Helix F, Helix F', Helix I, Helix I, Helix I, Helix I, K-K' loop, K-K' loop, C-terminal coil	(Bathelt et al., 2002)
	1DT6	Ifosfamide	**I114,** **F115,** **F206,** **I209,** L216, **S294,** **F297,** **A298,** **T302,** **L363,** **V367,** **V477**	B'-C loop, B'-C loop, Helix F, Helix F, Helix F', Helix I, Helix I, Helix I, Helix I, K-K' loop, K-K' loop, C-terminal coil	(Bathelt et al., 2002)
	1DT6	7-ethoxycoumarin	M103, **I209,** **L363,** **V367,** **V477**	B-B' loop, Helix F, K-K' loop, K-K' loop, C-terminal coil	(Spatzenegger et al., 2003)

	1DT6	4-trifluoromethyl-7-ethoxycoumarin	**S294,** **L363,** **V367,** **V477**	Helix I, K-K' loop, K-K' loop, C-terminal coil	(Spatzenegger et al., 2003)
	1DT6	7-pentoxyresorufin	**I114,** **F206,** S207, **T302,** **V367**	B'-C loop, Helix F, Helix F, Helix I, K-K' loop	(Lewis et al., 2004)
	1N6B	4-trifluoromethyl-7-ethoxycoumarin	**K100,** **I114,** **F115,** T205, **F206,** **T302,** **L363**	B-B' loop, B'-C loop, B'-C loop, Helix F, Helix F, Helix I, K-K' loop,	(Lewis et al., 2006)
CYP2B1[c]	N/A	3-cyclopentyloxy-*N*-(3,5-dichloro-4-pyridyl)-4-methoxybenzamide (RP 73401)	M103, R109, **L363,** M365, **V477**	B-B' loop, B'-C loop, K-K' loop, K-K' loop, C-terminal coil	(Domanski et al., 1999)
CYP2B4	Not Reported	Bergamottin	**A298,** **T302,** **L363**	Helix I, Helix I, K-K' loop	(Kent et al., 2006)
	1SUO	4-trifluoromethyl-7-ethoxycoumarin	**K100,** **I114,** **F115,** T205, **F206,** **T302,** **L363**	B-B' loop, B'-C loop, B'-C loop, Helix F, Helix F, Helix I, K-K' loop,	(Lewis et al., 2006)
	1SUO	Cyclophosphamide	**V104,** I110, **I114,** **F115,** **F206,** F208, **I209,** **F297,** **A298,** **E301,** **T302,** S320, **L363,** **V367,** **V477,** **G478**	B-B' loop, B'-C loop, B'-C loop, B'-C loop, Helix F, Helix F, Helix F, Helix I, Helix I, Helix I, Helix I, Helix J, K-K' loop, K-K' loop, C-terminal coil, C-terminal coil	(Nguyen et al., 2008)
	1SUO	4-(4-chlorophenyl) imidazole	**S210,** **F297,** **T302**	F-F' loop, Helix I, Helix I	(Lewis et al., 2010)

[a] Amino acids are numbered according to full-length refseq CYP2B6 (NX_P20813-1).
[b] Bolded and underlined amino acids indicate those found in the CYP2B6 active site according to the CYP2B6 crystal structures that have been solved and molecular docking results that have been yielded to date (Table 1).
[c] The CYP2B1 crystal structure utilized within Domanski et al., 1999 was homology modeled from a consensus of P450 BM-3, P450cam, and P450terp (Szklarz et al., 1995) and then used as a homology model for CYP2B6.

Supplemental Table 2. Kinetic parameters for the CYP2B6.1-mediated metabolism of substrates for which there are no reported catalytic constants of CYP2B6 mutants.

Substrate	Metabolic Method	Expression System[a]	K_m (μM)[a]	k_{cat} (min^{-1})[a]	Reference
Amitriptyline	*N*-demethylation	Human B-lymphoblastoid cell microsomes	144.4	NR	(Ekins and Wrighton, 1999)
Antipyrine	4-hydroxylation	Human B-lymphoblastoid cell microsomes	17,700	NR	(Ekins and Wrighton, 1999)
Arteether	*O*-deethylation	Human B-lymphoblastoid cell microsomes	28	NR	(Ekins and Wrighton, 1999)
Azinphos-methyl	*S*-oxidation	Supersomes	2.2	2.8	(Buratti et al., 2002)
2,2',4,4'-tetrabromodiphenyl ether (BDE-47)	3-hydroxylation	Supersomes	6.4	0.0106	(Feo et al., 2013)
	4-hydroxylation		2.7	0.150	(Erratico et al., 2013)
	4'-hydroxylation		1.2	0.270	(Erratico et al., 2013)
	5-hydroxylation		3.8	0.948	(Feo et al., 2013)
			5.8	0.300	(Erratico et al., 2013)
	6-hydroxylation		4.2	0.202	(Feo et al., 2013)
			2.8	0.260	(Erratico et al., 2013)
2,2',4,4',5-pentabromodiphenyl ether (BDE-99)	1'-hydroxylation	Supersomes	0.1	0.2116	(Erratico et al., 2012)
	2-hydroxylation		0.3	0.0068	(Erratico et al., 2012)
	4-hydroxylation		0.3	0.0276	(Erratico et al., 2012)
	4'-hydroxylation		0.9	0.2467	(Erratico et al., 2012)
	5'-hydroxylation		2.4	0.4573	(Erratico et al., 2012)
	6'-hydroxylation		0.3	0.0141	(Erratico et al., 2012)
2,2',4,4',6-pentabromodiphenyl ether (BDE-100)	3-hydroxylation	Supersomes	5.2	0.0099	(Gross et al., 2015)
	4'-hydroxylation		5.5	0.066	(Gross et al., 2015)
	5'-hydroxylation		4.9	0.166	(Gross et al., 2015)
	6'-hydroxylation		7.0	0.043	(Gross et al., 2015)
(R)-1,3-Benzodioxolyl-*N*-methylbutanamine (MBDB)	*N*-demethylation	Supersomes	138	2.5	(Niwa et al., 2011)
(S)-1,3-Benzodioxolyl-*N*-methylbutanamine (MBDB)			119	0.7	(Niwa et al., 2011)
(R)-1,3-Benzodioxolyl-*N*-methylbutanamine (MBDB)	Demethylenation		83	3.3	(Niwa et al., 2011)

(S)-1,3-Benzodioxolyl-*N*-methylbutanamine (MBDB)			56	0.2	(Niwa et al., 2011)
7-benzyloxyresorufin	*N*-demethylation	Human B-lymphoblastoid cell microsomes	1.28	NR	(Ekins and Wrighton, 1999)
7-benzyloxyquinoline	*O*-debenzylation	Baculovirus-infected insect cell microsomes	NR	0.55	(Renwick et al., 2001)
Bromoketamine	*N*-demethylation	Baculovirus-infected insect cell microsomes	10	94	(Wang et al., 2019)
4-chloromethyl-7-ethoxycoumarin	*O*-deethylation	Human B-lymphoblastoid cell microsomes	33.7	NR	(Ekins and Wrighton, 1999)
Carbaryl	Methyl hydroxylation	Supersomes	45	15.54	(Tang et al., 2002)
	4-hydroxylation		11	0.80	(Tang et al., 2002)
	5-hydroxylation		110	0.29	(Tang et al., 2002)
Cinnarizine	*p*-hydroxylation	Human B-lymphoblastoid cell microsomes	17.2	NR	(Ekins and Wrighton, 1999)
Clobazam	*N*-demethylation	Supersomes	289	5.70	(Giraud et al., 2004)
3-cyano-7-ethoxycoumarin	*O*-deethylation	Human B-lymphoblastoid cell microsomes	71.3	NR	(Ekins and Wrighton, 1999)
Deschloroketamine	*N*-demethylation	Baculovirus-infected insect cell microsomes	184	83	(Wang et al., 2019)
Dextromethorphan	*N*-demethylation	Human B-lymphoblastoid cell microsomes	350	NR	(Ekins and Wrighton, 1999)
Diazepam	*N*-demethylation	Human B-lymphoblastoid cell microsomes	181	NR	(Ekins and Wrighton, 1999)
Diazinon	*S*-oxidation	Supersomes	14.83	5.44	(Ellison et al., 2012)
	Dearylation		13.94	2.60	(Ellison et al., 2012)
1,2-dibromoethane	2-bromo acetaldehyde formation	Human B-lymphoblastoid cell microsomes	9,700	NR	(Ekins and Wrighton, 1999)
N,N-diethyl-m-toluamide (DEET)	Ring methyl hydroxylation	Supersomes	40.2	22.3	(Usmani et al., 2002)
			46.2	34.7	(Edwards et al., 2005)
Disulfoton	*S*-oxidation	Supersomes	11.2	62.2	(Usmani et al., 2004)
Efavirenz *trans*-alkene analog	7- or 8-hydroxylation	Supersomes	0.23	0.13	(Cox and Bumpus, 2014)

Efavirenz 13-propyl analog	5- or 7-hydroxylation and 8-hydroxylation		1.10	0.97	(Cox and Bumpus, 2014)
Efavirenz benzoxazine analog	7- or 8-hydroxylation		0.22	3.2	(Cox and Bumpus, 2014)
Efavirenz methyl benzoxazine analog	Methyl hydroxylation		1.4	NR	(Cox and Bumpus, 2016)
	5-, 7-, or 8-hydroxylation		1.0	NR	(Cox and Bumpus, 2016)
Efavirenz quinazolinone analog	Benzene ring hydroxylation		11	NR	(Cox and Bumpus, 2016)
Efavirenz *trans*-alkene quinazolinone analog	5-, 7-, or 8-hydroxylation		13	NR	(Cox and Bumpus, 2016)
Efavirenz quinolinone analog	Benzene ring hydroxylation		14	NR	(Cox and Bumpus, 2016)
Efavirenz benzo[d][1,3]dioxin-2-one analog	Unknown hydroxylation		5.5	NR	(Cox and Bumpus, 2016)
Endosulfan-α	*S*-oxidation	Supersomes	16.2	11.4	(Casabar et al., 2006)
			5.58	10.31	(Lee et al., 2006)
(-)-fenchone	6-exo-hydroxylation	Supersomes	150	12.9	(Miyazawa and Gyoubu, 2007)
	6-endo-hydroxylation		260	5.33	(Miyazawa and Gyoubu, 2007)
	10-hydroxylation		200	10.66	(Miyazawa and Gyoubu, 2007)
Fluoroketamine	*N*-demethylation	Baculovirus-infected insect cell microsomes	40	103	(Wang et al., 2019)
(R)-fluoxetine	*N*-demethylation	Supersomes	126	1.19	(Niwa et al., 2011)
(S)-fluoxetine			546	2.55	(Niwa et al., 2011)
7-hydroxyefavirenz	14-hydroxylation	Supersomes	62.4	1.3	(Ogburn et al., 2010)
8-hydroxyefavirenz	14-hydroxylation	Supersomes	2.12	8.5	(Ward et al., 2003)
			23.2	4.21	(Ogburn et al., 2010)
Ifosfamide	*N*-dechloro-ethylation	*Escherichia coli* C41 DE3	2,000	0.4	(Calinski et al., 2015)
	4-hydroxylation		4,600	3.8	(Calinski et al., 2015)
Deuterated ifosfamide[c]	*N*-dechloro-ethylation		2,000	0.2	(Calinski et al., 2015)
	4-hydroxylation		2,000	4.1	(Calinski et al., 2015)
(R)-ifosfamide	*N*-dechloro-ethylation	Supersomes	1,900	8.2	(Roy et al., 1999)
(S)-ifosfamide			900	11.8	(Roy et al., 1999)
(R)-ifosfamide	4-hydroxylation		NR	<0.4	(Roy et al., 1999)

			2,240	1.98	(Niwa et al., 2011)
(S)-ifosfamide			NR	2.08	(Roy et al., 1999)
			1,270	17.1	(Niwa et al., 2011)
Imipramine	*N*-demethylation	*Saccharomyces cerevisiae* microsomes	383	NR	(Ekins and Wrighton, 1999)
β-ionone	4-hydroxylation	Supersomes	5.6	572.8	(Marumoto et al., 2017)
Lidocaine	*N*-deethylation	Human B-lymphoblastoid cell microsomes	537.6	NR	(Ekins and Wrighton, 1999)
Loperamide	*N*-demethylation	Supersomes	65.6	0.008	(Kim et al., 2004)
Malathion	*S*-oxidation	Supersomes	3.09	3.6	(Buratti et al., 2005)
(S)-mephenytoin	*N*-demethylation	Human B-lymphoblastoid cell microsomes	564	NR	(Ekins and Wrighton, 1999)
(S)-mephobarbital	*N*-demethylation	Human B-lymphoblastoid cell microsomes	264	0.008	(Kobayashi et al., 1999a)
Methiocarb	*S*-oxidation	Supersomes	11.0	28.0	(Usmani et al., 2004)
Methyl parathion	*S*-oxidation	Supersomes	1.25	10.39	(Ellison et al., 2012)
	Dearylation		141	1.42	(Ellison et al., 2012)
Midazolam	1'-hydroxylation	Human B-lymphoblastoid cell microsomes	46.1	NR	(Ekins and Wrighton, 1999)
Naphthalene	1-hydroxylation	Supersomes	58.6	20.2	(Cho et al., 2006)
	2-hydroxylation		93.8	0.8	(Cho et al., 2006)
	1,2-dihydroxylation		49.5	2.2	(Cho et al., 2006)
Nevirapine	3-hydroxylation	Human B-lymphoblastoid cell microsomes	834	NR	(Erickson et al., 1999)
Nonane	2-hydroxylation	Supersomes	79.0	76.0	(Edwards et al., 2005)
2-nonanol	*C*-oxidation	Supersomes	35.0	72.8	(Edwards et al., 2005)
(R)-norketamine	5-hydroxylation	Supersomes	21.6[b]	16.72[b]	(Desta et al., 2012)
	C-oxidation		286.5	13.0	(Desta et al., 2012)
(S)-norketamine	5-hydroxylation		36.1[b]	16.3[b]	(Desta et al., 2012)
	C-oxidation		146.8	7.61	(Desta et al., 2012)

Parathion	*S*-oxidation	Supersomes	0.8	1.7	(Buratti et al., 2002)
		NR	0.61	4.827	(Foxenberg et al., 2007)
	Dearylation		0.74	1.804	(Foxenberg et al., 2007)
Pethidine	*N*-demethylation	Supersomes	262	82	(Murray et al., 2020)
Phorate	*S*-oxidation	Supersomes	32.1	70.8	(Usmani et al., 2004)
Propofol	4-hydroxylation	Human B-lymphoblastoid cell microsomes	10	21	(Court et al., 2001)
(-)-*cis*-rose oxide	9-hydroxylation	Supersomes	159.2	60.67	(Nakahashi et al., 2015)
(-)-*trans*-rose oxide			73.80	154.0	(Nakahashi et al., 2015)
Sertraline	*N*-demethylation	Human B-lymphoblastoid cell microsomes	30.7	2.04	(Kobayashi et al., 1999b)
(+)-*cis*-3,5-dimethyl-2-(3-pyridyl) thiazolidin-4-one hydrochloride (SM-12502)	*S*-oxidation	Human B-lymphoblastoid cell microsomes	1,767	NR	(Ekins and Wrighton, 1999)
Styrene	Glycol formation	Human B-lymphoblastoid cell microsomes	180	NR	(Ekins and Wrighton, 1999)
Verapamil	*O*-demethylation	Human B-lymphoblastoid cell microsomes	137.4	NR	(Ekins and Wrighton, 1999)

[a] NR indicates data/values that were not reported.
[b] These authors analyzed the diastereomeric metabolites formed by CYP2B6-mediated 5-hydroxylation of *(R;S)*-norketamine; CYP2B6 showed the highest intrinsic clearance with its production of *(2S,5S;2R,5R)*-hydroxynorketamine, the K_m and k_{cat} of which is reported.
[c] This ifosfamide was deuterated on its alpha and alpha' carbons.

REFERENCES

Bathelt C, Schmid RD, and Pleiss J (2002) Regioselectivity of CYP2B6: homology modeling, molecular dynamics simulation, docking. *J Mol Model* **8:**327-335.

Buratti FM, D'Aniello A, Volpe MT, Meneguz A, and Testai E (2005) Malathion bioactivation in the human liver: the contribution of different cytochrome p450 isoforms. *Drug Metab Dispos* **33:**295-302.

Buratti FM, Volpe MT, Fabrizi L, Meneguz A, Vittozzi L, and Testai E (2002) Kinetic parameters of OPT pesticide desulfuration by c-DNA expressed human CYPs. *Environ Toxicol Pharmacol* **11:**181-190.

Calinski DM, Zhang H, Ludeman S, Dolan ME, and Hollenberg PF (2015) Hydroxylation and N-dechloroethylation of Ifosfamide and deuterated Ifosfamide by the human cytochrome p450s and their commonly occurring polymorphisms. *Drug Metab Dispos* **43:**1084-1090.

Casabar RC, Wallace AD, Hodgson E, and Rose RL (2006) Metabolism of endosulfan-alpha by human liver microsomes and its utility as a simultaneous in vitro probe for CYP2B6 and CYP3A4. *Drug Metab Dispos* **34:**1779-1785.

Cho TM, Rose RL, and Hodgson E (2006) In vitro metabolism of naphthalene by human liver microsomal cytochrome P450 enzymes. *Drug Metab Dispos* **34:**176-183.

Court MH, Duan SX, Hesse LM, Venkatakrishnan K, and Greenblatt DJ (2001) Cytochrome P-450 2B6 is responsible for interindividual variability of propofol hydroxylation by human liver microsomes. *Anesthesiology* **94:**110-119.

Cox PM and Bumpus NN (2014) Structure-Activity Studies Reveal the Oxazinone Ring Is a Determinant of Cytochrome P450 2B6 Activity Toward Efavirenz. *ACS Med Chem Lett* **5:**1156-1161.

Cox PM and Bumpus NN (2016) Single Heteroatom Substitutions in the Efavirenz Oxazinone Ring Impact Metabolism by CYP2B6. *ChemMedChem* **11:**2630-2637.

Desta Z, Moaddel R, Ogburn ET, Xu C, Ramamoorthy A, Venkata SL, Sanghvi M, Goldberg ME, Torjman MC, and Wainer IW (2012) Stereoselective and regiospecific hydroxylation of ketamine and norketamine. *Xenobiotica* **42:**1076-1087.

Domanski TL, Schultz KM, Roussel F, Stevens JC, and Halpert JR (1999) Structure-Function Analysis of Human Cytochrome P-450 2B6 Using a Novel Substrate, Site-Directed Mutagenesis, and Molecular Modeling. *Journal of Pharmacology and Experimental Therapeutics* **290:**1141-1147.

Edwards JE, Rose RL, and Hodgson E (2005) The metabolism of nonane, a JP-8 jet fuel component, by human liver microsomes, P450 isoforms and alcohol dehydrogenase and inhibition of human P450 isoforms by JP-8. *Chem Biol Interact* **151:**203-211.

Ekins S and Wrighton SA (1999) The role of CYP2B6 in human xenobiotic metabolism. *Drug Metab Rev* **31:**719-754.

Ellison CA, Tian Y, Knaak JB, Kostyniak PJ, and Olson JR (2012) Human hepatic cytochrome P450-specific metabolism of the organophosphorus pesticides methyl parathion and diazinon. *Drug Metab Dispos* **40:**1-5.

Erickson DA, Mather G, Trager WF, Levy RH, and Keirns JJ (1999) Characterization of the in vitro biotransformation of the HIV-1 reverse transcriptase inhibitor nevirapine by human hepatic cytochromes P-450. *Drug Metab Dispos* **27:**1488-1495.

Erratico CA, Szeitz A, and Bandiera SM (2012) Oxidative metabolism of BDE-99 by human liver microsomes: predominant role of CYP2B6. *Toxicol Sci* **129:**280-292.

Erratico CA, Szeitz A, and Bandiera SM (2013) Biotransformation of 2,2',4,4'-tetrabromodiphenyl ether (BDE-47) by human liver microsomes: identification of cytochrome P450 2B6 as the major enzyme involved. *Chem Res Toxicol* **26:**721-731.

Feo ML, Gross MS, McGarrigle BP, Eljarrat E, Barcelo D, Aga DS, and Olson JR (2013) Biotransformation of BDE-47 to potentially toxic metabolites is predominantly mediated by human CYP2B6. *Environ Health Perspect* **121:**440-446.

Foxenberg RJ, McGarrigle BP, Knaak JB, Kostyniak PJ, and Olson JR (2007) Human hepatic cytochrome p450-specific metabolism of parathion and chlorpyrifos. *Drug Metab Dispos* **35:**189-193.

Giraud C, Tran A, Rey E, Vincent J, Treluyer JM, and Pons G (2004) In vitro characterization of clobazam metabolism by recombinant cytochrome P450 enzymes: importance of CYP2C19. *Drug Metab Dispos* **32:**1279-1286.

Gross MS, Butryn DM, McGarrigle BP, Aga DS, and Olson JR (2015) Primary role of cytochrome P450 2B6 in the oxidative metabolism of 2,2',4,4',6-pentabromodiphenyl ether (BDE-100) to hydroxylated BDEs. *Chem Res Toxicol* **28:**672-681.

Kent UM, Lin HL, Noon KR, Harris DL, and Hollenberg PF (2006) Metabolism of bergamottin by cytochromes P450 2B6 and 3A5. *J Pharmacol Exp Ther* **318:**992-1005.

Kim KA, Chung J, Jung DH, and Park JY (2004) Identification of cytochrome P450 isoforms involved in the metabolism of loperamide in human liver microsomes. *Eur J Clin Pharmacol* **60:**575-581.

Kobayashi K, Abe S, Nakajima M, Shimada N, Tani M, Chiba K, and Yamamoto T (1999a) Role of human CYP2B6 in S-mephobarbital N-demethylation. *Drug Metab Dispos* **27:**1429-1433.

Kobayashi K, Ishizuka T, Shimada N, Yoshimura Y, Kamijima K, and Chiba K (1999b) Sertraline N-demethylation is catalyzed by multiple isoforms of human cytochrome P-450 in vitro. *Drug Metab Dispos* **27:**763-766.

Lee HK, Moon JK, Chang CH, Choi H, Park HW, Park BS, Lee HS, Hwang EC, Lee YD, Liu KH, and Kim JH (2006) Stereoselective metabolism of endosulfan by human liver microsomes and human cytochrome P450 isoforms. *Drug Metab Dispos* **34:**1090-1095.

Lewis DF, Ito Y, and Goldfarb PS (2006) Investigating human P450s involved in drug metabolism via homology with high-resolution P450 crystal structures of the CYP2C subfamily. *Curr Drug Metab* **7:**589-598.

Lewis DF, Ito Y, and Lake BG (2010) Quantitative structure-activity relationships (QSARs) for inhibitors and substrates of CYP2B enzymes: importance of compound lipophilicity in explanation of potency differences. *J Enzyme Inhib Med Chem* **25:**679-684.

Lewis DF and Lake BG (1997) Molecular modelling of mammalian CYP2B isoforms and their interaction with substrates, inhibitors and redox partners. *Xenobiotica* **27:**443-478.

Lewis DF, Lake BG, and Dickins M (2004) Quantitative structure-activity relationships within a homologous series of 7-alkoxyresorufins exhibiting activity towards CYP1A and CYP2B enzymes: molecular modelling studies on key members of the resorufin series with CYP2C5-derived models of human CYP1A1, CYP1A2, CYP2B6 and CYP3A4. *Xenobiotica* **34:**501-513.

Lewis DF, Lake BG, Dickins M, Eddershaw PJ, Tarbit MH, and Goldfarb PS (1999) Molecular modelling of CYP2B6, the human CYP2B isoform, by homology with the substrate-bound CYP102 crystal structure: evaluation of CYP2B6 substrate characteristics, the

cytochrome b5 binding site and comparisons with CYP2B1 and CYP2B4. *Xenobiotica* **29:**361-393.

Lewis DF, Lake BG, Dickins M, and Goldfarb PS (2002) Molecular modelling of CYP2B6 based on homology with the CYP2C5 crystal structure: analysis of enzyme-substrate interactions. *Drug Metabol Drug Interact* **19:**115-135.

Marumoto S, Shimizu R, Tanabe G, Okuno Y, and Miyazawa M (2017) In Vitro Regio- and Stereoselective Oxidation of beta-Ionone by Human Liver Microsomes. *Planta Med* **83:**292-299.

Miyazawa M and Gyoubu K (2007) Metabolism of (-)-fenchone by CYP2A6 and CYP2B6 in human liver microsomes. *Xenobiotica* **37:**194-204.

Murray JL, Mercer SL, and Jackson KD (2020) Impact of cytochrome P450 variation on meperidine N-demethylation to the neurotoxic metabolite normeperidine. *Xenobiotica* **50:**209-222.

Nakahashi H, Yamamura Y, Usami A, Rangsunvigit P, Malakul P, and Miyazawa M (2015) Metabolism of (-)-cis- and (-)-trans-rose oxide by cytochrome P450 enzymes in human liver microsomes. *Biopharm Drug Dispos* **36:**565-574.

Nguyen TA, Tychopoulos M, Bichat F, Zimmermann C, Flinois JP, Diry M, Ahlberg E, Delaforge M, Corcos L, Beaune P, Dansette P, Andre F, and de Waziers I (2008) Improvement of cyclophosphamide activation by CYP2B6 mutants: from in silico to ex vivo. *Mol Pharmacol* **73:**1122-1133.

Niwa T, Murayama N, and Yamazaki H (2011) Stereoselectivity of human cytochrome p450 in metabolic and inhibitory activities. *Curr Drug Metab* **12:**549-569.

Ogburn ET, Jones DR, Masters AR, Xu C, Guo Y, and Desta Z (2010) Efavirenz primary and secondary metabolism in vitro and in vivo: identification of novel metabolic pathways and cytochrome P450 2A6 as the principal catalyst of efavirenz 7-hydroxylation. *Drug Metab Dispos* **38:**1218-1229.

Renwick AB, Lewis DF, Fulford S, Surry D, Williams B, Worboys PD, Cai X, Wang RW, Price RJ, Lake BG, and Evans DC (2001) Metabolism of 2,5-bis(trifluoromethyl)-7-benzyloxy-4-trifluoromethylcoumarin by human hepatic CYP isoforms: evidence for selectivity towards CYP3A4. *Xenobiotica* **31:**187-204.

Roy P, Tretyakov O, Wright J, and Waxman DJ (1999) Stereoselective metabolism of ifosfamide by human P-450s 3A4 and 2B6. Favorable metabolic properties of R-enantiomer. *Drug Metab Dispos* **27:**1309-1318.

Salonen JS, Nyman L, Boobis AR, Edwards RJ, Watts P, Lake BG, Price RJ, Renwick AB, Gomez-Lechon MJ, Castell JV, Ingelman-Sundberg M, Hidestrand M, Guillouzo A, Corcos L, Goldfarb PS, Lewis DF, Taavitsainen P, and Pelkonen O (2003) Comparative studies on the cytochrome p450-associated metabolism and interaction potential of selegiline between human liver-derived in vitro systems. *Drug Metab Dispos* **31:**1093-1102.

Spatzenegger M, Liu H, Wang Q, Debarber A, Koop DR, and Halpert JR (2003) Analysis of differential substrate selectivities of CYP2B6 and CYP2E1 by site-directed mutagenesis and molecular modeling. *J Pharmacol Exp Ther* **304:**477-487.

Szklarz GD, He YA, and Halpert JR (1995) Site-directed mutagenesis as a tool for molecular modeling of cytochrome P450 2B1. *Biochemistry* **34:**14312-14322.

Tang J, Cao Y, Rose RL, and Hodgson E (2002) In vitro metabolism of carbaryl by human cytochrome P450 and its inhibition by chlorpyrifos. *Chem Biol Interact* **141:**229-241.

Usmani KA, Karoly ED, Hodgson E, and Rose RL (2004) In vitro sulfoxidation of thioether compounds by human cytochrome P450 and flavin-containing monooxygenase isoforms with particular reference to the CYP2C subfamily. *Drug Metab Dispos* **32:**333-339.

Usmani KA, Rose RL, Goldstein JA, Taylor WG, Brimfield AA, and Hodgson E (2002) In vitro human metabolism and interactions of repellent N,N-diethyl-m-toluamide. *Drug Metab Dispos* **30:**289-294.

Wang PF, Neiner A, Lane TR, Zorn KM, Ekins S, and Kharasch ED (2019) Halogen Substitution Influences Ketamine Metabolism by Cytochrome P450 2B6: In Vitro and Computational Approaches. *Mol Pharm* **16:**898-906.

Wang Q and Halpert JR (2002) Combined three-dimensional quantitative structure-activity relationship analysis of cytochrome P450 2B6 substrates and protein homology modeling. *Drug Metab Dispos* **30:**86-95.

Ward BA, Gorski JC, Jones DR, Hall SD, Flockhart DA, and Desta Z (2003) The cytochrome P450 2B6 (CYP2B6) is the main catalyst of efavirenz primary and secondary metabolism: implication for HIV/AIDS therapy and utility of efavirenz as a substrate marker of CYP2B6 catalytic activity. *J Pharmacol Exp Ther* **306:**287-300.